Tectonics®

RESEARCH ARTICLE
10.1029/2024TC008374

Special Collection:
Alpine mountain belts in 4-dimensions

Post-Collisional Reorganisation of the Eastern Alps in 4D – Crust and Mantle Structure

Peter J. McPhee[1] and **Mark R. Handy**[1,2]

[1]Institute of Geological Sciences, Freie Universität Berlin, Berlin, Germany, [2]Institute of Geological Sciences, Universität Bern, Bern, Switzerland

Abstract The Eastern Alps were affected by a profound post-collisional tectonic reorganisation in Neogene time, featuring indentation by the Adriatic upper plate, rapid uplift and filling of the eastern Molasse Basin, exhumation and eastward orogen-parallel transport of Paleogene metamorphic units in the orogenic core, and a shift from northward thrust propagation in the European plate to southward propagation in the Adriatic plate. We test the idea that these events were triggered by slab detachment by reconstructing the indentation process. This involves sequentially restoring N-S and E-W cross-sections of the orogenic wedge and correcting for out-of-section orogen-parallel transport with a map-view reconstruction. We propose two phases of indentation: Initially (23 and 14 Ma), the whole Adriatic crust acted as an indenter. Its northward motion was accommodated by upright folding and orogen-parallel extensional exhumation in the Tauern Window. This phase was followed (14 Ma to Present) by continued orogen-parallel transport of the orogenic wedge into the Pannonian Basin and deformation of the leading edge of the Adriatic indenter, forming the Southern Alps fold-thrust belt. The lower crust of the Southern Alps indented the base of the Venediger Nappes in the Tauern Window, forming a high-velocity (6.8–7.25 km/s) ridge in map view at 30–45 km depth. By correlating the post-23 Ma orogenic evolution with presently imaged European slab segments in P-wave teleseismic tomography, we discern two possible Neogene slab removal events: One from 23 to 19 Ma triggering tectonic reorganisation of the Eastern Alps and its foreland basin, and potentially a second event after 14 Ma.

Key Points:

- The Eastern Alps were first indented by Adriatic lithosphere (23 and 14 Ma), then by Adriatic lower crust as the indenter deformed (14 and 0 Ma)
- Shortening of the orogenic wedge since 23 Ma requires 135 km of subduction and 90 km of eastward extrusion of orogenic lithosphere
- Slab detachment at 23 and 20 Ma and possibly after 14 Ma is constrained by areal balancing of crust and mantle

Supporting Information:

Supporting Information may be found in the online version of this article.

Correspondence to:

P. J. McPhee,
peter.mcphee@fu-berlin.de

Citation:

McPhee, P. J., & Handy, M. R. (2024). Post-collisional reorganisation of the Eastern Alps in 4D – Crust and mantle structure. *Tectonics*, *43*, e2024TC008374. https://doi.org/10.1029/2024TC008374

Received 22 APR 2024
Accepted 24 JUN 2024

Author Contributions:

Conceptualization: Peter J. McPhee, Mark R. Handy
Formal analysis: Peter J. McPhee
Funding acquisition: Mark R. Handy
Investigation: Peter J. McPhee, Mark R. Handy
Methodology: Peter J. McPhee
Supervision: Mark R. Handy
Visualization: Peter J. McPhee
Writing – original draft: Peter J. McPhee
Writing – review & editing: Peter J. McPhee, Mark R. Handy

1. Introduction

Slab detachment, also known as break-off, is a commonly invoked process affecting the post-collisional evolution of orogenic belts. In this paper, we sometimes use the term *slab removal* as a more neutral, non-mechanistic term to describe the elimination of subducted lithosphere from beneath orogens. By whatever means, releasing the slab-pull force is predicted to drive uplift (e.g., Buiter et al., 2002; Duretz et al., 2011; Wortel & Spakman, 2000), reshaping orogens and their peripheral basins (e.g., Fox et al., 2015; Sinclair, 1997). Slab remnants that have detached and sunk into the mantle have been widely imaged in seismic tomography, particularly below orogenic belts (e.g., van der Meer et al., 2018; Wortel & Spakman, 2000). Yet, discerning the geological signals of slab removal above these remnants, particularly uplift, is challenging because processes such as crustal shortening and erosion may conceal them. Moreover, a scarcity of high-resolution geophysical data and an incomplete picture of orogenic evolution often complicates detailed examination of the relationship between subduction, orogenesis, and slab detachment. Together, these uncertainties have driven much discussion and controversy surrounding the role of slab removal in the Alps and beyond (e.g., Garzanti et al., 2018; Kästle et al., 2020; McPhee et al., 2022). Recently, the Eastern Alpine crust and mantle have been seismologically imaged in unprecedented detail using a network of over 600 temporary broadband stations deployed during the *AlpArray* passive array experiment (2015–2019, AlpArray Seismic Network Team et al., 2018; average station spacing of 40 km), as well as an even denser targeted array of 163 stations over the Eastern and eastern Southern Alps (Swath D, average station spacing of 15 km, Heit et al., 2023). P-wave teleseismic models reveal high-velocity anomalies interpreted as subducted and partly detached slabs (Handy et al., 2021; Paffrath et al., 2021). In contrast to classical ideas of subduction in collisional settings that involve horizontally continuous slabs and single detachment events (e.g., von Blanckenburg & Davies, 1995), positive slab anomalies below the Eastern Alps have a non-cylindrical structure with vertical and horizontal gaps (e.g., Handy et al., 2021; Malusà et al., 2021). If AlpArray-derived teleseismic models represent the mantle structure accurately, they may demonstrate a complex history of orogen-parallel slab segmentation, potentially with more than one slab removal event.

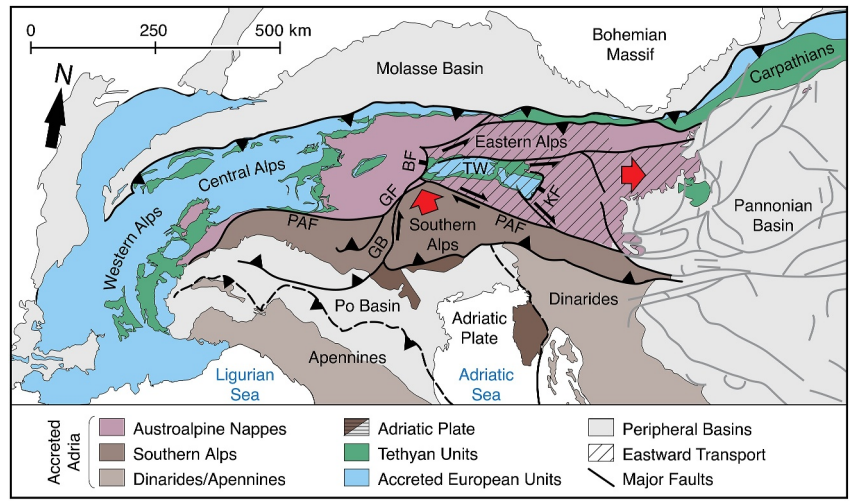

Figure 1. Tectonic map of the Alps and surrounding basins and mountain belts (redrawn after Handy et al., 2019; Schmid et al., 2004). BF—Brenner Fault; GB—Giudicarie Belt; GF—Giudicarie Fault; KF—Katschberg Fault; PAF—Periadriatic Fault; TW—Tauern Window.

Unlike the Western and Central Alps, north-directed orogenesis in the Eastern Alps was significantly modified by orogen-parallel transport of the orogenic wedge in Neogene times (e.g., Frisch et al., 2000; Ratschbacher et al., 1991; Scharf et al., 2013; Schmid et al., 2013; Wölfler et al., 2011). Those events broadly coincided with a switch in orogenic polarity from north-directed thrusting in the Eastern Alps to south-directed thrusting in the Southern Alps (Handy et al., 2023), as well as rapid infilling and coeval tectonic uplift of the eastern Molasse Basin (Genser et al., 2007; Le Breton et al., 2023).

In using the term Eastern Alps, we refer specifically to part of the orogenic edifice east of the Brenner Fault and north of the Giudicarie and Periadriatic Faults (Figure 1, hatched area bounded by lines labeled BF, GF, and PAF) that experienced N- to NW-directed indentation by the eastern Southern Alps in latest Oligocene to Miocene time. This usage is more specific from the standpoint of Neogene tectonics and differs from broader definitions of Eastern Alps that refer either geographically to the part of the Alps east of Switzerland, or geologically to that part of the Alps with an intact cover of Austroalpine Nappes overlying the Paleogene nappe stack (Schmid et al., 2004, colored purple in Figure 1).

By reconstructing the structural evolution of the indented and east-transported Eastern Alps during Neogene time, we attempt to correlate crustal structure with the mantle structure revealed by teleseismic P-wave tomography (Paffrath et al., 2021). We restore Neogene deformation along two orogen-normal cross-sections—the well-known TRANSALP transect at ~12°E (e.g., Lüschen et al., 2004) that is based on controlled-source seismology (CSS), and the *Eastern Alpine Seismological Initiative* (EASI) transect at 13.3°E (e.g., Hetényi et al., 2018), a passive-array swath experiment conducted in an early stage of the *AlpArray* project. In addition, we present an E-W orogen-parallel cross-section that intersects the TRANSALP and EASI transects (Figure 2). We use local earthquake tomography (LET) to investigate the structure and fate of the lower crust during the switch from north-to south-directed thrusting across the orogen. To make the balancing of Neogene tectonics truly three-dimensional, the effects of eastward transport in the N-S cross-sections are accounted for using a map-view reconstruction. We use these balanced cross-sections to constrain the timing and kinematics of indentation, as well as to infer the mechanical response of both indented and indenting crust during slab removal.

2. Geological Setting

The Eastern Alps comprise rocks derived from the Adriatic continental upper plate (Austroalpine Nappes), the subducted European continental lower plate (Tauern Window) and the accreted remains of the Mesozoic Alpine Tethyan Ocean (Alpine Tethys) that once separated these continents (Figure 1). Subduction of the Alpine Tethys in Late Cretaceous time was followed by an Adria-Europe continental collision in the late Eocene, marked by the

10.1029/2024TC008374

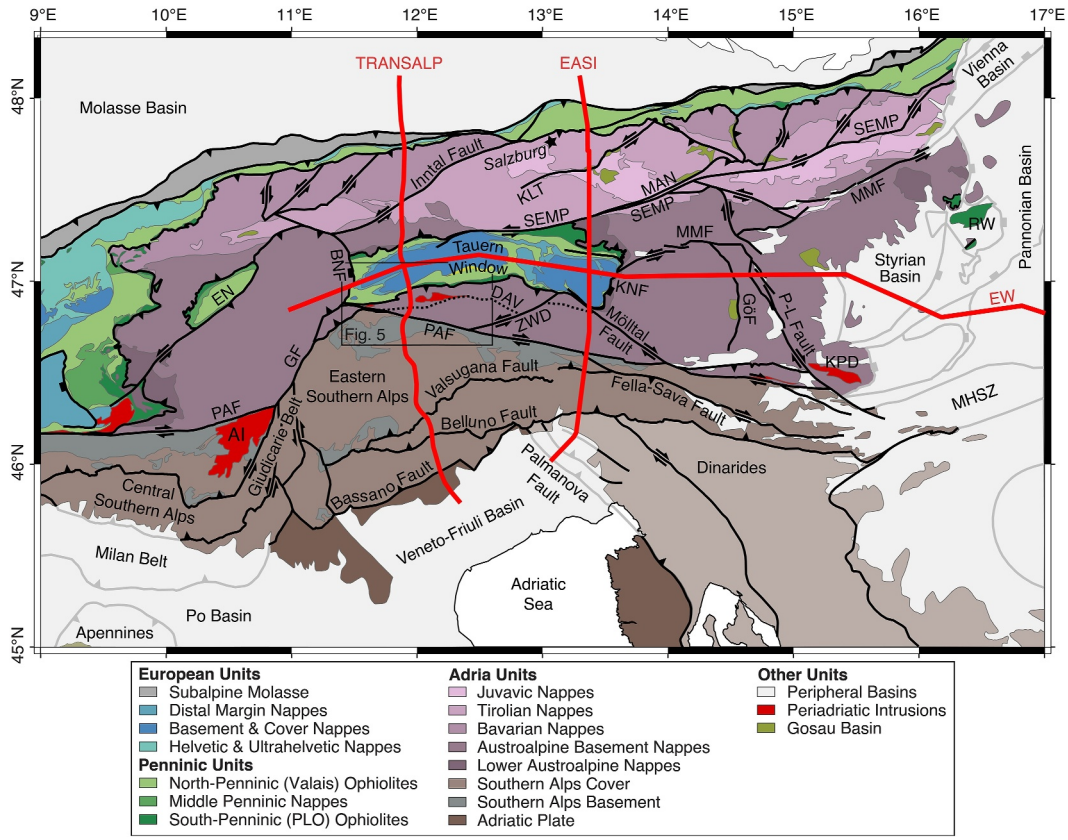

Figure 2. Tectonic map of the Central and Eastern Alps based on Schmid et al. (2004) and faults from McPhee et al. (in prep). Thick red lines indicate traces of the TRANSALP, EASI, and EW cross-sections in this study. Abbreviations: AI—Adamello Intrusion; DAV—Defereggen-Anterselva/Antholz-Valles/Vals Fault; BF—Brenner Fault; EN—Engadin Window; GF—Giudicarie Fault; GöF—Görschitztal Fault; KLT—Königsee-Lammertal-Traunsee Fault; KF—Katschberg Fault; KPD—Kozak and Pohorje Domes; MAN—Mandling Fault; MHSZ—Mid Hungarian Shear Zone; MMF—Mur-Mürz Fault; PAF—Periadriatic Fault; P-L—Pöls-Lavanttal; RW—Rechnitz Window; SEMP—Salzach-Ennstal-Mariazell-Puchberg Fault; ZWD—Zwischenbergen-Wöllatratten-Drau Fault.

incorporation of distal European passive margin units into the orogenic wedge and deposition of orogen-derived sediments on the European foreland.

The Molasse Basin forms the northern foreland basin of the Eastern Alps and holds a record of the erosion and northward advance of the Alpine orogen with respect to Europe (Figure 2). East of the TRANSALP cross-section (Figure 2) the Molasse Basin experienced deep marine deposition from ~25 to 19 Ma, followed by coeval rapid infilling and tectonic uplift from 19 to 17 Ma (e.g., Hülscher et al., 2019; Kuhlemann & Kempf, 2002). The Subalpine Molasse comprises folded and thrusted slices of the Molasse Basin and is the northernmost and structurally lowest tectonic unit along the northern front of the Eastern Alps (e.g., Ortner et al., 2022). In the Eastern Alps, thrusting of the Subalpine Molasse advanced northward until early Miocene time, when the thrusts were sealed by lower Miocene (Aquitanian-Burdigalian, 23–20 Ma) strata in the western part of the eastern Molasse Basin (i.e., west of Salzburg, Figure 2; Hinsch, 2013). After that, only minor out-of-sequence deformation affected the northern orogenic front and thrusting stepped back into the orogen (Ortner et al., 2014).

The Helvetic Nappes, structurally above the Subalpine Molasse, comprise Permo-Mesozoic sedimentary rocks derived from the former European passive margin of Alpine Tethys (e.g., Pfiffner, 1993). These nappes are poorly exposed along the Eastern Alpine orogenic front and are intercalated with equally poorly exposed thrust slices of the structurally-higher Penninic Nappes. The Penninic Nappes consist of ophiolites derived from the subducted Alpine Tethys (e.g., Kurz et al., 1996; Schmid et al., 2004). In the Tauern Window, where the Penninic Nappes are best exposed, they record Paleogene high-pressure and subsequent high-temperature metamorphism (e.g., Hoinkes et al., 1999; Schuster et al., 2004).

The Austroalpine Nappes are the structurally highest nappes in the Alps and are derived from the Adriatic Plate (e.g., Schmid et al., 2004). Nappe stacking occurred during the Cretaceous Eoalpine Orogeny. During subsequent subduction of the Alpine Tethyan Ocean and Adria-Europe collision, this older nappe stack formed a lid that was affected by further shortening during Paleogene collision and nappe stacking (e.g., Handy et al., 2010). Across the Eastern Alps, the Austroalpine Nappes are unconformably overlain by outliers of the Late Cretaceous to Paleogene syn-to post-orogenic sediments of the Gosau Basins (Figure 2; e.g., Wagreich & Faupl, 1994).

On the northern side of the Eastern Alps, the Austroalpine Nappes include the far-traveled, weakly- to non-metamorphic Northern Calcareous Alps (Figure 2), which were accreted in Cretaceous time from the northern margin of the Neotethyan ocean (Frisch & Gawlick, 2003; Schmid et al., 2004). The structurally underlying Austroalpine Basement Nappes are best exposed to the south of the Northern Calcareous Alps and comprise pre-Alpine basement and cover that experienced Late Cretaceous mid-temperature and high-pressure metamorphism during the Eoalpine orogeny (e.g., Hoinkes et al., 1999; Schuster et al., 2004).

The Tauern Window exposes subducted, accreted, and metamorphosed units of the European passive margin (the sub-Penninic Venediger Nappes) and overlying Penninic Nappes. The Venediger Nappes comprise a thrust duplex of basement slices separated by thinned Permo-Mesozoic cover rocks (e.g., Groß et al., 2020, 2022). These underwent high-pressure metamorphism in Paleogene time (e.g., Handy & Oberhänsli, 2004; Liu et al., 2001) before the entire thrust duplex was overprinted by high-temperature, Barrovian-type metamorphism at peak conditions of 620°C, 0.7 GPa at 28–30 Ma (e.g., Favaro et al., 2015).

The Tauern Window (Figure 2) is bounded to the W and E by oppositely dipping, low-angle normal faults (Brenner and Katschberg faults, respectively) and to the N and S by conjugate strike-slip faults. Together, these faults accommodated E-W extension and E-directed orogen-parallel motion of the Eastern Alpine orogenic crust (Figure 1; e.g., Frisch et al., 2000; Linzer et al., 2002; Ratschbacher et al., 1989, 1991; Rosenberg et al., 2018; Scharf et al., 2013). Our cross-sections (Figure 4, traces in Figure 2) transect these strike-slip faults.

Cooling of the Venediger Nappes began in the Oligo-Miocene (∼28–23 Ma) and accelerated in early to middle Miocene time (∼23–9 Ma, e.g., (Favaro et al., 2015; Fügenschuh et al., 1997; Luth & Willingshofer, 2008; Wölfler et al., 2012). This cooling has been attributed to exhumation involving a combination of broadly coeval upright post-nappe folding, erosion, and extensional exhumation in the footwalls of the Brenner and Katschberg normal faults (Bertrand et al., 2017; Favaro et al., 2017; Rosenberg et al., 2018; Scharf et al., 2013).

The Southern Alps fold-thrust belt, located south of the Periadriatic Fault, comprises non-metamorphic Permo-Mesozoic cover and basement derived from Adria (e.g., Bertotti et al., 1993; Winterer & Bosellini, 1981). Unlike the Austroalpine Nappes, the nappes of the Southern Alps verge to the south to southeast and comprise mostly sediments that are in close proximity with their basement substratum. The eastern Southern Alps are separated from the central and western parts of the Southern Alps by the Giudicarie Belt (Figure 1), an oblique sinistral transpressional fold-thrust belt (e.g., Picotti et al., 1995; Verwater et al., 2021) which, together with the NNE-SSW-trending Giudicarie Fault, was active in early-to-late Miocene time (Castellarin, Vai, & Cantelli, 2006; Pomella et al., 2011, 2012). The Giudicarie Belt sinistrally offsets the Periadriatic Fault and Oligocene Periadriatic intrusive rocks (marked red in Figure 2), subdividing the Adriatic indenter into the Ivrea (western) and Dolomites (eastern) subindenters (e.g., Handy et al., 2015; Rosenberg et al., 2018). In the eastern Southern Alps, thrust faults rooting in the basement formed since middle Miocene times, as dated by the youngest (lower-to-middle Miocene) sedimentary rocks in their footwalls (Castellarin et al., 1998; Verwater et al., 2021, and references therein). This age is corroborated by evidence for flexural deepening of the Veneto-Friuli Basin (Mellere et al., 2000) and by thermal modeling of cooling ages along eroded hangingwall anticlines above thrust faults (Eizenhöfer et al., 2023). The thrusts in the easternmost Southern Alps offset older SW-directed thin-skinned thrusts of the Late Cretaceous-to Paleogene Dinaric fold-thrust belt (e.g., Merlini et al., 2002; Poli & Zanferrari, 2018; Ponton, 2010). West of the Giudicarie Belt, Miocene thrusting affecting the basement was preceded by an earlier phase (Late Cretaceous or Paleogene?) of thrusts crosscut by the Oligocene Adamello intrusion (e.g., Brack, 1981; Schönborn, 1992).

3. Tomographic Models of the Eastern and Southern Alps

A dense network of temporary stations of the AlpArray and SWATH-D experiments at a node spacing of 5–15 km (Jozi Najafabadi et al., 2022) allows us to use LET to visualize the P-wave velocity structure down to 60 km depth.

10.1029/2024TC008374

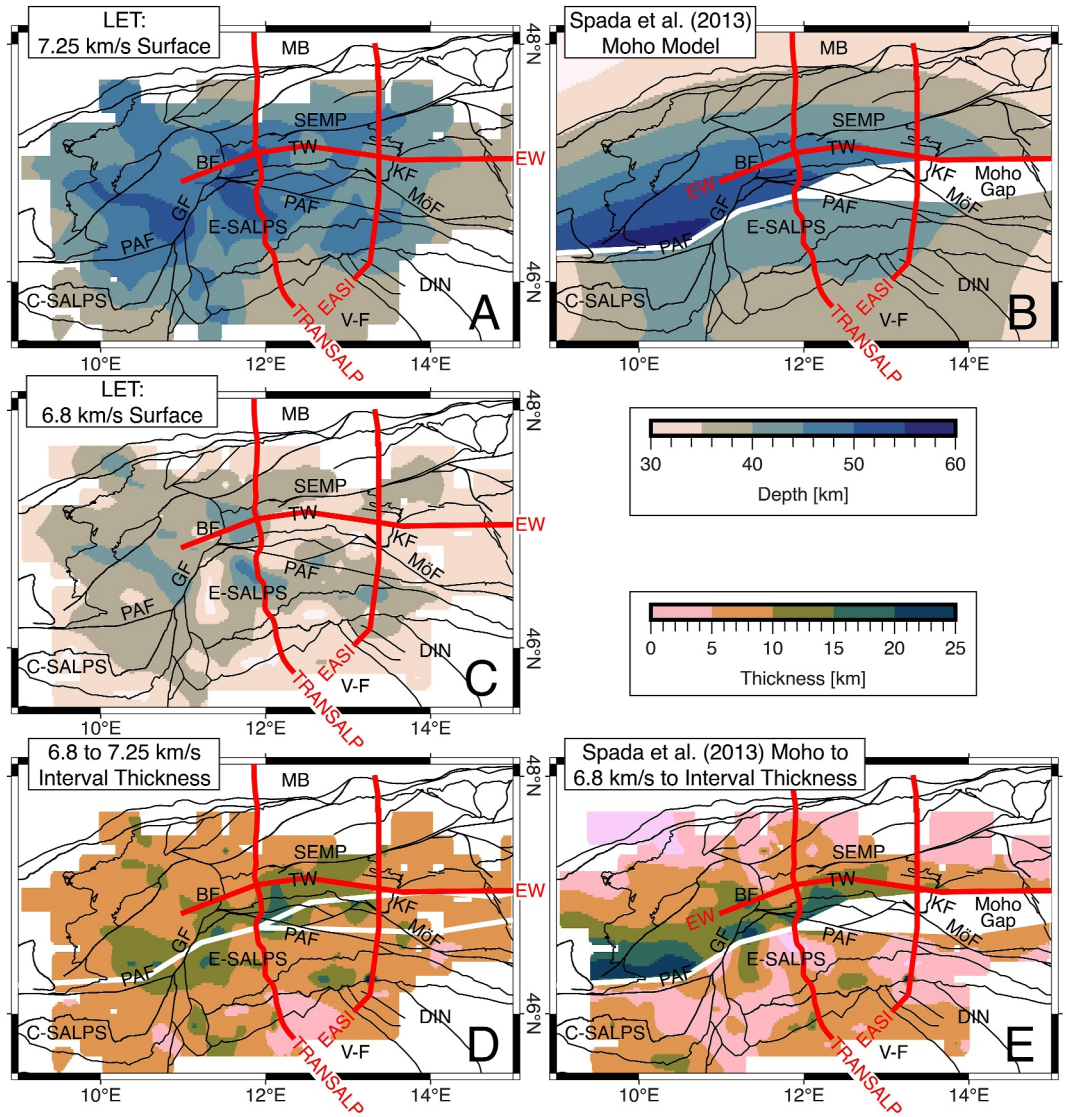

Figure 3. LET data and Moho model across the Eastern Alps, with black lines defining major thrusts and strike-slip faults. The upper color bar shows depths to these surfaces, and the lower colourbar shows thickness between surfaces. Abbreviations: BF—Brenner Fault; DIN—Dinarides; KF—Katschberg Fault; MB—Molasse Basin; MöF—Mölltal Fault; GF—Giudicarie Fault; PAF—Periadriatic Fault; C-SALPS—central Southern Alps; E-SALPS—eastern Southern Alps; SEMP—Salzach-Ennstal-Mariazell-Puchberg Fault; TW—Tauern Window; V-F—Veneto-Friuli Basin (See Figure 2 for additional labels). (a) 7.25 km/s (Moho proxy) isovelocity surfaces from Jozi Najafabadi et al. (2022). (b) Spada et al. (2013) Moho model. (c) 6.8 km/s (top lower crust proxy) isovelocity surfaces from Jozi Najafabadi et al. (2022). (d) 7.25 to 6.8 km/s interval thickness, interpreted to represent lower crustal thickness. (e) 6.8 km/s (top lower crust proxy) isovelocity surface to Spada et al. (2013) Moho model.

P-wave velocities reflect the bulk physical properties of rock averaged over a volume roughly proportional to the spacing between seismic stations at the surface. Although LET is a truly 3D method that yields potentially high-resolution and reliable 3D velocity information for consistent data sets, LET models do not directly reproduce velocity discontinuities such as the Moho or crustal-scale faults, instead resolving these as smooth velocity gradients.

In the LET model of Jozi Najafabadi et al. (2022), the Moho in Figure 3a is defined by a proxy velocity value of 7.25 km/s, an average of lower crustal and upper mantle velocities. For comparison, Figure 3b shows the Moho map of Spada et al. (2013) based on a weighted combination of Moho depth estimates from LET, Receiver Function (RF), and controlled-source seismic (CSS) methods. The white area in Figure 3b indicates where no

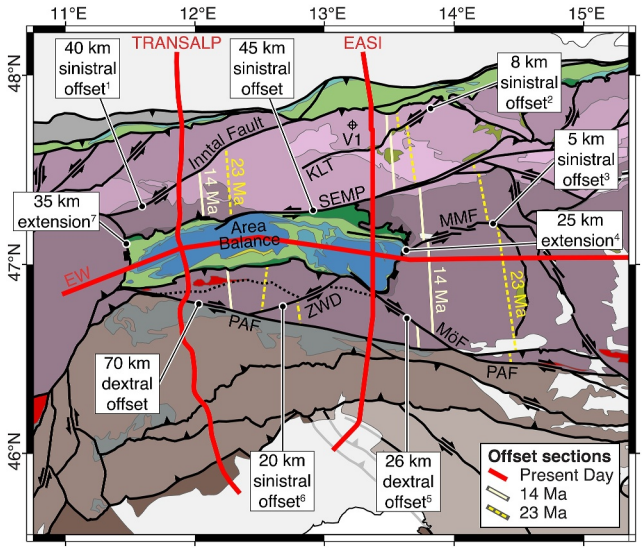

Figure 4. Part of Figure 2 showing the offset cross-sections used to correct for the effects of eastward orogen-parallel transport. These were located using the a map-view reconstruction based on total strike-slip offset estimates from: (1) Inntal Fault—Ortner et al. (2006); (2) KLT—Königsee-Lammertal-Traunsee—Linzer et al. (2002); (3) MMF—Mur-Mürz Fault—Eder and Neubauer (2000); (4) KF—Katschberg Fault—Scharf et al. (2013); (5) MöF—Mölltal Fault (Favaro et al., 2017); (6) ZWD—Zwischenbergen-Wöllatratten-Drau Fault—Favaro et al. (2017); (7) BF—Brenner Fault—Wolff et al. (2021). Neogene SEMP Fault displacement (45 km) is obtained by balancing the effects of extension on the Katschberg Fault and the E-W lengthening of the Austroalpine units south of the Tauern Window that was accommodated by the ZWD and Mölltal faults. Periadriatic Fault displacement is assumed to accommodate the eastward transport of these units. V 1 is the location of the Vordersee 1 borehole (Brix & Schultz, 1993). See Figure 2 for the legend.

Moho could be imaged due to a low velocity gradient (Diehl et al., 2009). Thus, we define the Moho in our cross-sections in Figure 4 as the mean trace of available Moho models along each geophysical transect (LET—Jozi Najafabadi et al., 2022; Diehl et al., 2009; RF—Bianchi et al., 2021; Hetényi et al., 2018; Kummerow et al., 2004; Mroczek et al., 2023; joint inversion of LET, RF, and CSS—Spada et al., 2013).

The boundary between lower and intermediate crust is taken to be a proxy velocity of 6.8 km/s (Figure 3c), corresponding to an average of P-wave velocities measured in the laboratory on exhumed crustal rocks from the Ivrea-Verbano Zone in the western-most Southern Alps (Figure 1; Burke & Fountain, 1990). There, a complete section of the Southern Alps (Adriatic) crust exposes non-metamorphic Permo-Mesozoic sedimentary rocks in the southeast to intermediate crustal, lower crustal, and upper mantle rocks in the northwest (Zingg et al., 1990). The rocks in the Ivrea section are typical of both the Adriatic and European lower crust because they share a common late Palaeozoic and Early Mesozoic history before the opening of Alpine Tethys (e.g., Handy et al., 1999).

To determine the thickness of the lower crust, we subtract the depths of the 6.8 km/s (Figures 3c) from the 7.25 km/s isovelocity surfaces (Figure 3a) and the Moho model of Spada et al. (2013) (Figure 3b). The resulting thickness maps (Figures 3d and 3e) show that in the Central Alps west of the Giudicarie Fault, the lower crust is thickened north of the Periadriatic Fault. East of the Giudicarie Fault, a thick ridge of lower crust runs subparallel to the Giudicarie Fault beneath the Southern Alps, then continues northward to beneath the SW corner of the Tauern Window, where it attains its greatest thickness. The Moho is not offset by the Giudicarie Belt and Giudicarie Fault (Figures 3a and 3b), suggesting this major fault system is confined to the crust. In the eastern Southern Alps, the 6.8 km/s isovelocity surface deepens from the Veneto-Friuli Basin toward the Periadriatic Fault (Figure 3c). North of the Periadriatic Fault and beneath the Tauern Window, the 6.8 km/s isovelocity surface shallows to the north and east.

4. Section Construction and Reconstruction Approach

We construct our cross-sections in the structural modeling and analysis software *Move*™ 2019, assuming minimum shortening. Where available, we use and adapt existing subsurface interpretations. We link structures exposed at the surface to the LET and Moho models in the subsurface. Along the TRANSALP cross-section, we use reflectors manually picked from vibroseis- and dynamite-source seismic data in Lüschen et al. (2006).

In the Neogene, the Eastern Alps were transected by dextral and sinistral strike-slip faults that facilitated eastward orogen-parallel transport of the orogenic wedge (Figures 1 and 2; e.g., Bartosch et al., 2017; Favaro et al., 2017; Linzer et al., 2002; Ratschbacher et al., 1991; Robl et al., 2008; Rosenberg et al., 2018; Wölfler et al., 2011). In our north-south-oriented cross-sections, this transport violates the basic assumption of plane strain made in 2D balancing (i.e., motion only in the plane of the cross-section). To address this, we utilize a map-view reconstruction to restore out-of-section transport at 23 and 14 Ma (Figure 4). We choose these periods to represent the initiation of accelerated cooling of the Venediger Nappes, related to extension and upright folding (23 Ma) and to represent the onset of south-directed thrusting in the eastern Southern Alps (14 Ma). We first retrodeform the map-view reconstruction to the timesteps of interest, drawing straight cross-section traces that connect the EASI and TRANSALP cross-sections from the European foreland to the Southern Alps. We then forward-model the map-view reconstruction, translating segments of the 14 and 23 Ma cross-sections to their present locations (colored segments in Figure 4). Finally, we interpret the present structure in the offset cross-section traces. We assemble them into composite cross-sections representing the orogen at 14 and 23 Ma. Our composite cross-sections maintain the present-day cross-sectional area of the accreted European units exposed in the Tauern Window.

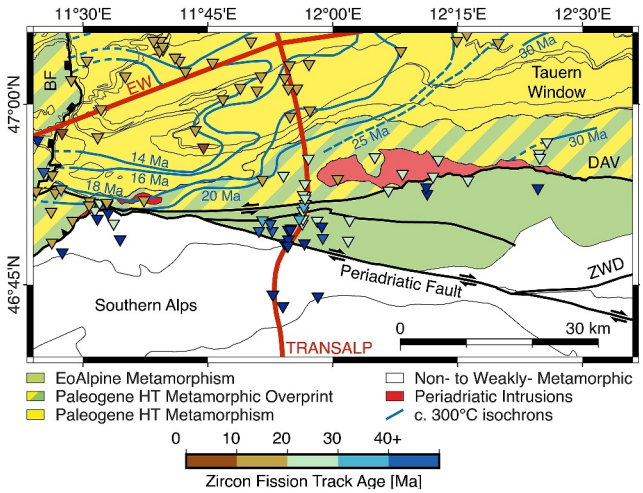

Figure 5. Map of the southwestern Tauern Window showing where the Periadriatic Fault cuts the S-dipping Paleogene nappe contacts (taken here from Schmid et al., 2013) as well as Paleogene high temperature (HT) metamorphism (Schuster et al., 2004) and Neogene isochrons related to post-nappe cooling and exhumation. Blue contours are 300°C cooling isochrons from Handy and Oberhänsli (2004), based on a compilation of biotite Rb-Sr and Ar-Ar white mica cooling ages. Zircon fission track ages compiled from Bertrand et al. (2017), Elias (1998), Fügenschuh (1995), Klotz et al. (2019), Most (2003), Pomella et al. (2012), Steenken et al. (2002), Stöckhert et al. (1999), Viola et al. (2001). BF—Brenner Fault; DAV—Defereggen-Anterselva/Antholz-Valles/Vals Fault; ZWD—Zwischenbergen-Wöllatratten-Drau Fault.

5. Present Structure

Figure 6 shows the present orogenic structure of the Eastern Alps in three cross-sections that depict key structural features. These cross-sections form the basis of the retrodeformation that follows, where we demonstrate that our cross-sections are balanced and kinematically viable.

5.1. TRANSALP

Along the TRANSALP cross-section (TRANSALP Working Group, 2002), the segment between the Molasse Basin and the DAV Fault (Figure 2) is based on existing structural interpretations across the Subalpine Molasse and Penninic and Helvetic nappes (Ortner et al., 2014), the Northern Calcareous Alps to the Inntal Fault (Auer & Eisbacher, 2003) and between the Inntal Fault and Tauern Window (Ortner et al., 2006). A package of seismic reflectors dips gently southward from the foreland, marking the Penninic and Helvetic nappes and Permo-Mesozoic cover of the European crust below the Northern Calcareous Alps (Figure 6a). Following previous interpretations (e.g., Lüschen et al., 2006), we link these reflectors to the Adriatic Moho along a ramp beneath the Tauern Window, the *Sub-Tauern Ramp*. This major thrust runs parallel to south-dipping seismic reflectors at the base of the Venediger Nappes. Receiver function models of the Moho along the TRANSALP cross-section (Kummerow et al., 2004; Mroczek et al., 2023) show that the European Moho dips south beneath the Adriatic Moho and is separated from the latter by a vertical gap. We interpret this gap to represent subducted European crust, corresponding to a positive anomaly in the local earthquake (Figure 6a; Jozi Najafabadi et al., 2022) and teleseismic P-wave tomographic images (Figure 7a; Handy et al., 2021; Paffrath et al., 2021).

Following the near-surface structural interpretation of Schmid et al. (2013; their cross-section 3) across the Tauern Window to the DAV, we link the Penninic Nappes at the surface to moderately south-dipping seismic reflectors at 14–18 km depth (e.g., TRANSALP Working Group et al., 2002). This package of reflectors is sub-parallel to reflectivity in the adjacent Austroalpine Nappes and Southern Alps basement and terminates abruptly down-dip, leading us to interpret a fault offset that we link vertically upwards to the surface trace of the Periadriatic Fault (marked PAF in Figure 6a). We interpret the Venediger, Penninic, and Austroalpine nappes as continuing southwards at depth, forming a south-tapering wedge of intermediate crust below the Southern Alps (Figure 6a).

Our interpretation of the Periadriatic Fault in the TRANSALP cross-section is consistent with observations at the surface that show this fault is a brittle structure that obliquely cuts the folded contacts between the Austroalpine, Penninic, and Venediger nappes, and truncates Neogene cooling age contours (Figure 5) at the southwest corner of the Tauern Window (Handy et al., 2005; Klötz et al., 2019; Luth & Willingshofer, 2008). Slip along this fault was right-lateral, with only a few kilometres of north-side up motion during the late Oligocene and Miocene (Luth & Willingshofer, 2008; Mancktelow et al., 2001; Ratschbacher et al., 1991). Therefore, the Periadriatic Fault post-dates not only nappe formation but also most of the Oligo-Miocene exhumation of these nappes. The main foliation parallel to the steeply S-dipping nappe contacts cut by the Periadriatic Fault accommodated the bulk of shearing related to nappe exhumation since 30 Ma (≤25 km, Handy et al., 2005, their Figure 5 and references therein). In Figure 6a, this foliation is interpreted to correspond to the S-dipping reflectors that continue at depth to the south beneath the Southern Alps.

Our interpretation of the deep structure of the TRANSALP cross-section (Figure 6a) differs from interpretations of the TRANSALP Working Group (2002) in which the contacts between the Venediger, Penninic, and Austroalpine nappes, as well as the Periadriatic Fault at the surface were extrapolated to depth in very different ways: (a) S-dipping and concordant with the south-dipping reflectors (their Model A) and; (b) steeply to N-dipping and discordant with these reflectors (their Model B, see also Castellarin, Nicolich, et al., 2006). In the second scenario, the Periadriatic Fault was inferred to connect with the Sub-Tauern Ramp to accommodate vertical exhumation and eastward lateral transport of the metamorphic units exposed in the Tauern Window. Interpretations since then

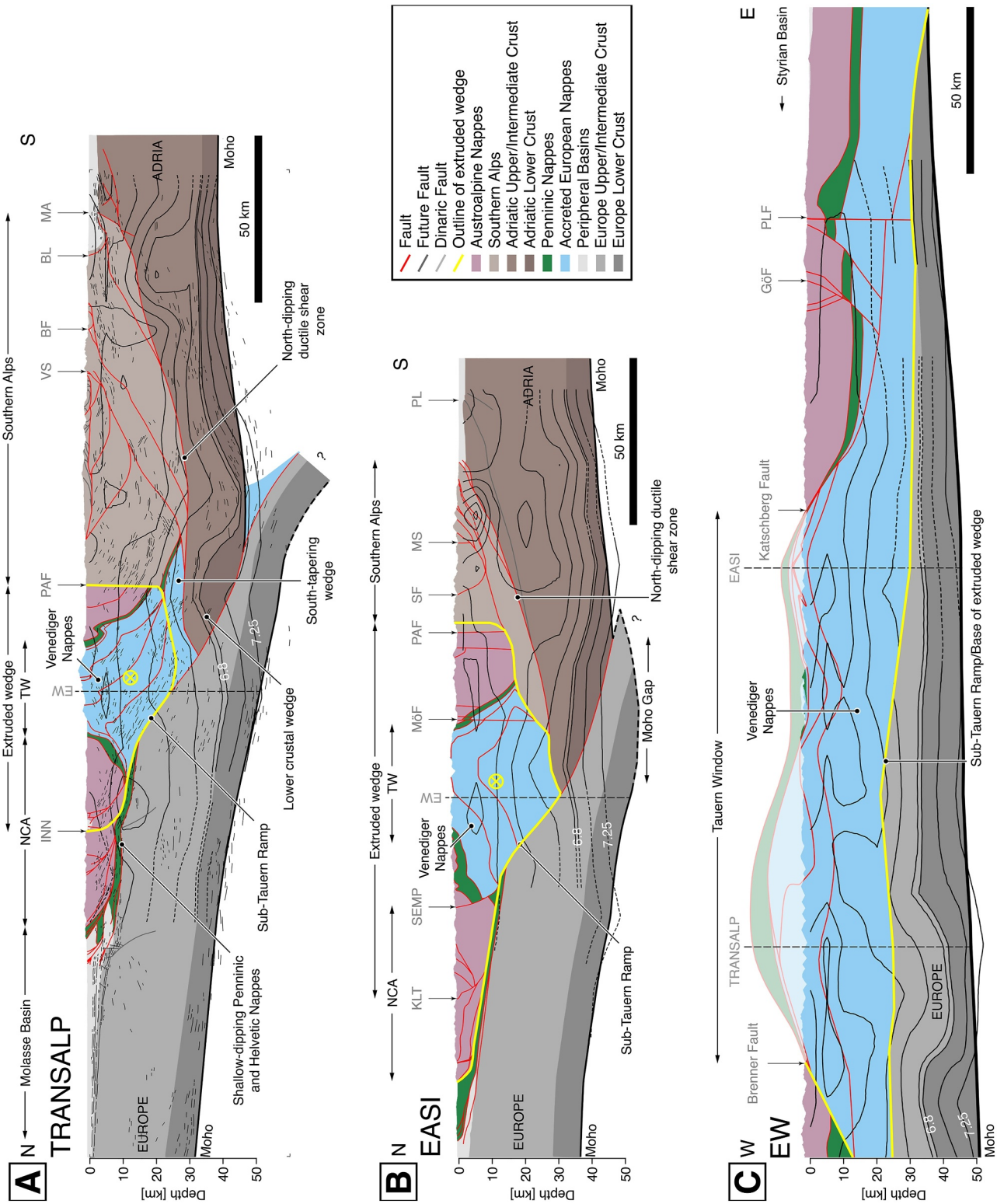

Figure 6. Present structure along the TRANSALP (a), EASI (b), and EW (orogen-parallel) cross-sections (c), all shown at the same scale. In the EW cross-section (c), the Venediger and Penninic Nappes are projected above the surface, based on the cross-sections of Schmid et al. (2013). Cross-section traces in map-view are shown in Figure 2. LET contours at 0.25 km/s intervals on the sections are from Jozi Najafabadi et al. (2022). BL—Bassano Anticline; BF—Belluno Fault; GöF—Görschitztal Fault; IN—Inntal Fault; KLT—Königsee-Lammertal-Traunsee Fault; MA—Montello Anticline; MöF—Mölltal Fault; MS—Monte Simone Fault; NCA—Northern Calcareous Alps; PAF—Periadriatic Fault; SEMP—Salzach-Ennstal-Mariazell-Puchberg Fault; PLF—Pöls Lavanttal Fault; SF—Sava-Fella Fault; TW—Tauern Window; VS—Valsugana Fault.

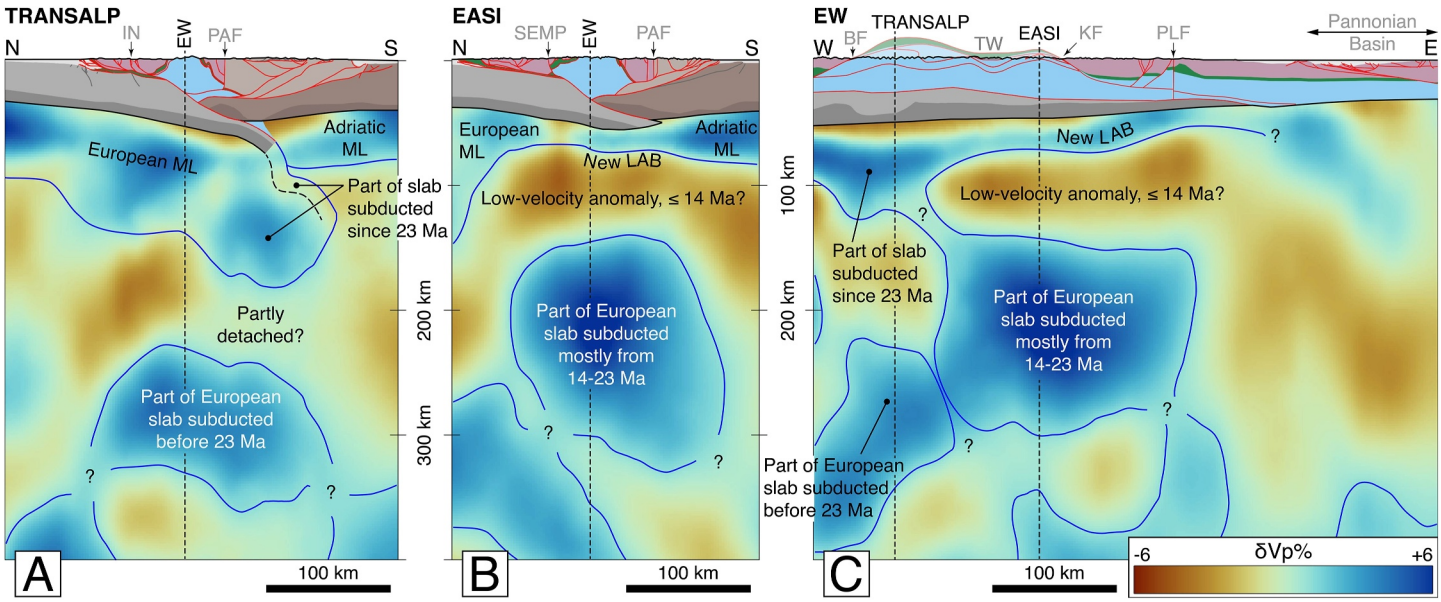

Figure 7. Structural model along the TRANSALP, EASI, and EW cross-sections, in relation to P-wave teleseismic tomography (Paffrath et al., 2021; we followed the common approach of smoothing model voxels using linear interpolation). The EW cross-section reaches eastward to the Pannonian Basin, as defined by Miocene graben structures underlying the Plio-Pleistocene cover (see map trace in Figure 2). Dashed dark gray lines mark intersections of the cross-sections. The blue lines closely follow the +1% anomaly contour line and outline the interpreted boundary between lithospheric and asthenospheric mantle. ML—Mantle lithosphere. The blue line subdividing the large positive anomaly in C is drawn according to geological criteria (see Section 7.3). Domains marked with "?" may be attributed to compositional variability and/or smearing of the image of the downgoing European lithospheric mantle. Labels indicating interpreted mantle structures are described in Section 7.3. See Figure 2 for cross-section traces in map view and Figure 6 for labeled structures in cross-sections. BF—Brenner Fault; IN—Inntal Fault; PAF—Periadriatic Fault; PLF—Pöls-Lavanttal Fault.

have adopted variants of these two end-member models (e.g., Rosenberg et al., 2018; Schmid et al., 2004, 2013), with most authors adopting variations of the TRANSALP B "lateral extrusion" model. Unfortunately, the deep structure of the Periadriatic Fault remains virtually unconstrained despite repeated efforts to address the challenge of imaging discrete subvertical structures with low impendence contrasts (e.g., 3D-Kirckhoff stack migration—Bleibinhaus & Groschup, 2008; Seismic diffraction imaging—Bauer et al., 2024). A subvertical Periadriatic Fault that connects at depth with a detachment surface beneath the Tauern Window (Figure 6a) is consistent with surface field observations and satisfies the kinematic necessity of accommodating coeval N-S shortening and eastward lateral extrusion in Neogene time.

South of the Periadriatic Fault, we reconstruct the Southern Alps fold-thrust belt using 1:50,000 and 1:100,000 geological maps published by the Geological Survey of Italy (see supplementary materials) and incorporate the structural interpretations of the Montello and Bassano anticlines in Picotti et al. (2022; Figure 6a) based on reprocessed seismic reflection, borehole, and surface geological data. Along TRANSALP, the Southern Alps are deformed from north to south by the Valsugana Fault, Belluno Fault, Bassano Anticline, and Montello Anticline (Figures 2 and 6a).

In the hangingwall of the Valsugana Fault, a thin-skinned fold-thrust belt deforms the Upper Permian to Cretaceous cover sequence of the Dolomites, with the evaporite-bearing Upper Permian Bellerophon Formation serving as a basal decollement. This formation is squeezed out along thrusts and in the cores of anticlines. We link part of this shortening to subsurface thrusts reaching into the basement. Most of the thrusts in the hangingwall of the Valsugana Fault are older SW-directed thrusts of the Dinaric fold-thrust belt (e.g., Castellarin & Cantelli, 2000; Doglioni & Bosellini, 1987).

The Dolomites are affected by open folds and an overall gentle north-dipping to subhorizontal regional dip (e.g., Castellarin et al., 1998). To reproduce this shallow regional dip above the stacked Valsugana, Belluno, Bassano, and Montello thrust faults, we find that the thick-skinned thrusts must link into a north-dipping ductile shear zone. This reaches down to 15–20 km depth, below the Bassano and Montello anticlines, and is associated with the deepest seismicity in the area (e.g., Anderlini et al., 2020). Such a ductile shear zone was previously proposed in

balanced cross-sections (Nussbaum, 2000; Schönborn, 1999; Verwater et al., 2021) and thermo-kinematic models of the Southern Alps fold-thrust belt (Eizenhöfer et al., 2023).

As mentioned above, LET models of the Eastern Alpine crust consistently show an upward perturbation or bulge of velocity contours on the southern side of the Tauern Window (Diehl et al., 2009; Jozi Najafabadi et al., 2022). In map view, this bulge forms an E-W trending high-velocity structure some 5–10-km-high and oriented sub-parallel to the Eastern Alps just south of the Tauern Window (Figure 3d). In the TRANSALP cross-section (Figure 6a), this high-velocity bulge is located south of and below the Tauern Window, below the Periadriatic Fault and north of the Moho gap.

5.2. EASI

We use the cross-section of Hinsch (2013; their Figure 8a) through the Subalpine Molasse, and Penninic and Helvetic nappes, which is based on borehole data and depth-migrated 3D seismic reflection data. From the front of the Northern Calcareous Alps to the Periadriatic Fault, we construct the cross-section in Figure 6b using 1:50,000 geological maps published by the Austrian Geological Survey (GeoSphere Austria; see supplementary materials). In the Northern Calcareous Alps, we incorporate the Vordersee-1 borehole (Brix & Schultz, 1993; Figure 4), which reached the buried Penninic and Helvetic nappes. Analogous to the TRANSALP cross-section, we reconstruct these nappes above a south-dipping decollement as far south as the SEMP Fault (Figures 2 and 6b). We assume that the regional dip of this thrust mimics that of the European Moho.

The SEMP sinistral strike-slip fault marks the southern limit of the Northern Calcareous Alps in the EASI cross-section. It juxtaposes the lowest Austroalpine and underlying Penninic nappes with the structurally higher Northern Calcareous Alps (Figure 6b). Between the SEMP and Tauern Window, folded Penninic rocks exposed to the west of the EASI cross-section (Figure 2) lead us to interpret a thin cover of Austroalpine Basement rocks that plunge steeply south at the SEMP Fault to form a north-dipping monocline. We interpret this monocline as the foreland-dipping limb of a fault-bend fold, marking the location of the subsurface Sub-Tauern Ramp. In contrast to the TRANSALP cross-section where the European and Adriatic Mohos are separated by a vertical gap (Figure 6a), the Moho along the EASI cross-section is poorly defined in the vicinity of the Tauern Window and beneath the Periadriatic Fault (Figure 3b), for the reasons pointed out above.

Our orogen-normal cross-section of the Venediger Nappes in the Tauern Window closely resembles those of Schmid et al. (2013) and Rosenberg et al. (2018). Figure 6b shows an open, upright fold in the Tauern Window with a vertical to overturned upper contact in the shallow subsurface that attains a shallower dip at depth.

The high-velocity bulge situated above the Moho gap, just south of the Tauern Window and below the Periadriatic Fault decreases in amplitude going eastward from the TRANSALP to the EASI cross-sections (Figures 3e, 6a, and 6b). This may reflect a thinner lower crust and shallower Moho toward the east. We take the Moho gap to define the southern end of the European slab (e.g., Hetényi et al., 2018; Spada et al., 2013), which is directly underlain by a high-velocity anomaly in LET and teleseismic P-wave tomographic models, and then by a negative velocity anomaly in P-wave tomography (Handy et al., 2021; Paffrath et al., 2021).

To define the structure south of the Periadriatic Fault in the Southern Alps, we modify the cross-section of Ponton (2010), which incorporates seismic interpretations and borehole data of Merlini et al. (2002). Seismicity down to 15–20 km in the actively deforming, frontal part of the Southern Alps indicates that, as in the TRANSALP cross-section, thrusting is linked to shear zones deeply rooted in the basement (e.g., Bressan et al., 2016). A NE-SW segment of this cross-section allows balancing of orogen-normal shortening relative to the autochthonous Adriatic foreland. We extend the Ponton (2010) cross-section north to the Periadriatic Fault based on the large-scale geological map of the Friuli-Venezia-Giulia region (Battista Carulli et al., 2006). There, we interpret a south-dipping monocline between the Periadriatic and Sava-Fella faults (marked PAF and S-F respectively, in Figure 6b) where Palaeozoic sedimentary, volcanic, and basement rocks are exposed adjacent to the Periadriatic Fault. Our cross-section shows two major thrusts in the basement that splay upwards into the marly, locally gypsum-bearing Upper Triassic Raibl Formation to form a thrust imbricate.

The EASI cross-section includes the E-W striking Sava-Fella Fault (Figure 2, marked S-F in Figure 6b). A dextral offset of some 30–60 km has been proposed along the Slovenian segment of this fault based on a visual correlation of Oligocene volcanic rocks (e.g., Fodor et al., 1998). West of the EASI cross-section (Figure 2), this fault accommodates N-S shortening and subordinate dextral motion and terminates at a compressive horsetail structure

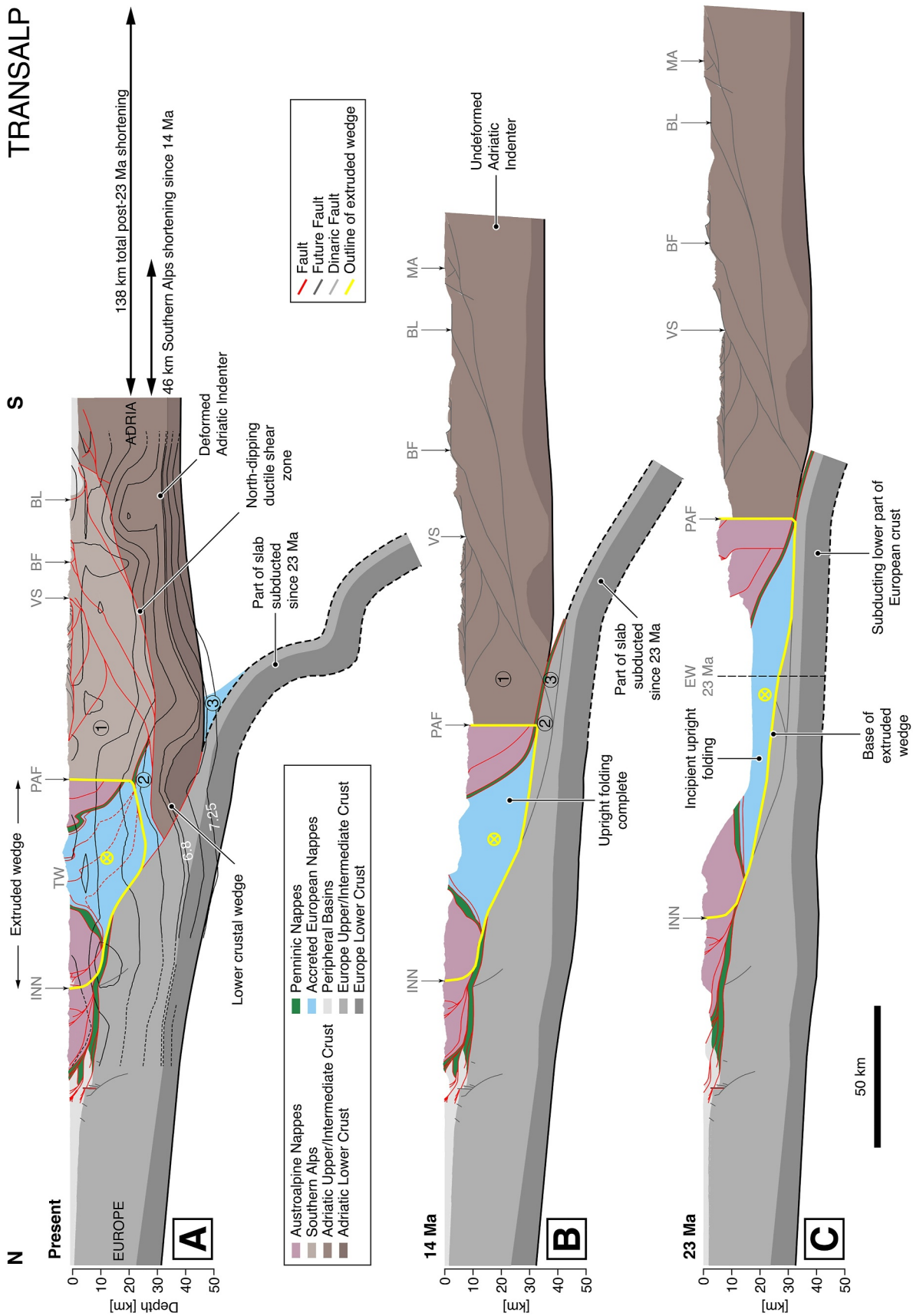

Figure 8. Restoration of the TRANSALP cross-section from the Present (a) back to 14 Ma (b) and 23 Ma (c). The slab geometry in A is based on P-wave teleseismic tomography (Figure 7). The length of the restored part of the slab is that required to underpin the Venediger Nappes at 23 Ma, and is maintained from 23 Ma to present, illustrating the amount of European subduction since 23 Ma. LET velocity contours at intervals of 0.25 km/s are taken from Jozi Najafabadi et al. (2022). Oblique-slip faults bounding the eastward extruding wedge are highlighted in yellow.

(Bartel et al., 2014). Based on its hangingwall and footwall geometries, we reconstruct the Sava-Fella Fault—in Figure 6b as a subvertical south-dipping dextral-oblique thrust with minor associated fault splays (Jadoul & Nicora, 1986) that root in the basement (Merlini et al., 2002; Moulin & Benedetti, 2018; Nussbaum, 2000; Ponton, 2010).

Toward the foreland of the Southern Alps, Dinaric structures are unconformably covered by synorogenic sedimentary rocks of late Cretaceous to Paleogene age (Merlini et al., 2002) indicating that these structures were not significantly reactivated during Neogene deformation. North of the frontal thrusts, these sediments are absent, and so we rely on detailed structural analysis of Ponton (2010) to identify Dinaric thrust faults. Geological markers indicate a maximum of about 5 km of dextral offset across the system of Dinaric strike-slip faults (Moulin et al., 2016; see also Žibret & Žibret, 2023). This is consistent with estimates of up to 1 km from 1:50,000 scale geological map (Zanferrari et al., 2013) of associated fault splays. We modify the interpretation of Ponton (2010) to depict the Monte Simone Fault as a strike-slip fault (marked MS in Figure 6b; Zanferrari et al., 2013), thereby removing an interpreted structural repetition of Mesozoic sedimentary rocks along a shallow-dipping Monte Simone Thrust (Merlini et al., 2002; Moulin & Benedetti, 2018).

5.3. EW (Orogen-Parallel)

In the E-W orogen-parallel cross-section from the Central Alps to the Pannonian Basin (Figure 6c), we use the Moho model of Spada et al. (2013), which closely matches the Moho proxy (7.25 km/s) in the LET model of Jozi Najafabadi et al. (2022). In the hangingwall of the Brenner Fault, we project west-plunging structures from the surface into the cross-section and tie our interpretation to the NW-SE cross-section of Pomella et al. (2016; their Figure 3b). Across the Tauern Window, we use a series of N-S and E-W oriented cross-sections from Schmid et al. (2013) and Groß et al. (2022) and augment our interpretation of the shallow-subsurface structure with structural information from tectonic contacts at the surface. In the hangingwall of the Katschberg Fault, we use 1:50,000 scale geological maps published by the Austrian Geological Survey (GeoSphere; see supplementary materials for details), projecting tectonic contacts down- or up-dip into the cross-section. Finally, in the Styrian and Pannonian Basins (shown only in Figure 7c), we project the interpretation of the seismic reflection survey in Maros et al. (2012) onto our cross-section.

Two features of the orogen-parallel cross-section in Figure 6c stand out: (a) the eastward shallowing of the Moho from ∼50 km below the Central Alps to ∼35 km below the Styrian Basin, and even less to the east below the Pannonian Basin (Figure 3b); and (b) the anomalous thickness of European-derived crust in the Tauern Window. This crust is thinned to the west and east in the footwalls of the Brenner and Katschberg normal faults, respectively. Comparing the orogen-parallel and orogen-normal cross-sections, it is interesting to note that the anomalous thickness of intermediate European crust beneath the Tauern Window occurs immediately above and to the north of the lower crustal bulge overlying the gap between the Adriatic and European Mohos (Figures 6a–6c).

5.4. Present Mantle Structure

In Figure 7, we augment our model of the crustal structure with the P-wave teleseismic tomographic model of Paffrath et al. (2021) that images the upper mantle structure. A multitude of P-wave tomographic models are available for the Alpine and Carpathian domains (e.g., Bijwaard & Spakman, 2000; Karousova et al., 2013; Koulakov et al., 2009, 2009; Lippitsch, 2002; Serretti & Morelli, 2011; Zhu et al., 2015), but we chose Paffrath et al. (2021) because it uses three existing crustal velocity models (Diehl et al., 2009; Kennett et al., 1995; Tesauro et al., 2008) to arrive at an optimized crustal correction (see Paffrath et al., 2021 and their supplement for description). The high resolution afforded by this model is crucial for imaging structures in the depth interval of 60–150 km, which includes the transition from the orogenic crust to the lithospheric slabs beneath the Alps.

Positive velocity anomalies are generally interpreted as cooler and denser mantle lithosphere that either forms the base of the orogenic lithosphere and/or reaches further down as a slab into the asthenosphere. The asthenosphere is generally considered warmer and, therefore, marked by negative anomalies. However, we cannot rule out compositional heterogeneities as the cause of local variations in velocity (Figure 7a).

In the TRANSALP cross-section, the European lithosphere extends southwards beneath the orogenic lithosphere to at least 200 km (Figure 7a) depth. In contrast, no high-velocity slab anomaly is observed beneath the EASI

cross-section (Figure 7b). The latter cross-section is marked by a discontinuity in the orogenic lithosphere between the European and Adriatic sides. This pronounced east-west change in the mantle structure in the TRANSALP and EASI cross-sections is best seen in the orogen-parallel cross-section (Figure 7c), where the slab anomaly in the TRANSALP cross-section gives way to the east to a low-velocity anomaly below the Tauern Window at a depth interval of approximately 70–150 km. This anomaly broadens from 12.5°E eastward toward the Pannonian Basin. The 1% velocity anomaly contour outlining the slab illustrates that the slab is largely disconnected from the overlying orogenic lithosphere.

6. Retrodeformation

6.1. TRANSALP

In the 14 Ma cross-section (Figure 7b), we restore 46 km of N-S shortening in the Southern Alps fold-thrust belt above a north-dipping ductile shear zone. The shortened upper to middle crustal rocks are interpreted to have formed the cover of the Adriatic lower crustal wedge, which is imaged as a high-velocity anomaly in the LET data (Figures 3 and 8). In the present-day cross-section (Figure 7a), we interpret a south-tapering wedge of European crust (Figures 8a and 8b, thrust slice labeled [2]) between the Adriatic lower crustal wedge and the Southern Alps (Figure 8a, thrust slice labeled [1]). This out-of-sequence stacking of units is achieved by inferring that the Valsugana Fault cut down to the north and accreted this slice of European crust. Serravallian (∼14–12 Ma) conglomerates preserved in its footwall (Castellarin et al., 1992) constrain thrusting to have occurred no earlier than 14 Ma.

We restore 17 km of N-S shortening accommodated by eastward orogen-parallel motion between the Periadriatic and Inntal faults (Figure 4) from 14 to 0 Ma (Figure 8b). North of the Inntal Fault, the Subalpine Molasse was shortened by 8 km from 23 to 9 Ma (Ortner et al., 2014). We assume that this was accommodated at a constant rate (0.6 km/Myr) and thus restore 3 km of shortening from 14 to 9 Ma. Adding this shortening to the 46 km shortening in the Southern Alps detailed above, we estimate up to 66 km of shortening in the TRANSALP cross-section since 14 Ma.

Going further back in time from 14 to 23 Ma, we restore 21 km of N-S shortening associated with orogen-parallel motion (Figure 8c) including sinistral motion along the ZWD related to E-W stretching of the Austroalpine Nappes between the Tauern Window and Periadriatic Fault (Figure 2; Favaro et al., 2017; Scharf et al., 2013). In the Tauern Window, the Venediger Nappes were affected by ductile folding and shearing under retrograde amphibolite-to-greenschist-facies conditions (Favaro et al., 2015). We restore 30 km of shortening by upright folding, treating the Venediger Nappes as a single unit with a fixed cross-sectional area. These nappes experienced E-W stretching, which in a N-S cross-section is represented by area loss. In the absence of constraints on the magnitude of this loss, we assume constant area, thereby slightly underestimating the actual area that the Venediger Nappes would have occupied in the TRANSALP cross-section at 23 and 14 Ma.

In the Tauern Window, the Austroalpine Nappes that once formed the roof of the Venediger Nappes have been eroded (Favaro et al., 2017), so we calculate the vertical distance to the top of the Venediger Nappe stack at 23 Ma by using estimates of maximum burial (20 km) from geobarometry in post-nappe Barrovian metamorphism (0.7 GPa, Selverstone, 1993). Finally, we restore the European lower crust from the Sub-Tauern Ramp, south of and below the unfolded Venediger Nappes (Figures 8a and 8c). We restore 22 km of shortening north of the Inntal Fault, including 5 km in the Subalpine Molasse. Taken together, the amount of N-S shortening between 23 and 14 Ma in the TRANSALP cross-section amounts to 72 km. Thus, the total N-S shortening since 23 Ma is 138 km.

We note that the balancing of the TRANSALP cross-section necessitates subducting a small piece of intermediate European crust (labeled [3] in Figure 8a). In the absence of seismological evidence for this fragment, we arbitrarily placed it in the mantle wedge immediately south of the Moho gap between the European and Adriatic Plates. However, its precise location is unimportant for the purposes of this reconstruction.

6.2. EASI

In the 14 Ma cross-section (Figure 9b), we restore 49 km of shortening in the Southern Alps above a north-dipping ductile shear zone that forms the base of the deformed part of the Adriatic indenter. As in the TRANSALP cross-section, the shortened upper and middle crustal rocks of the Southern Alps fold-and-thrust belt originally formed

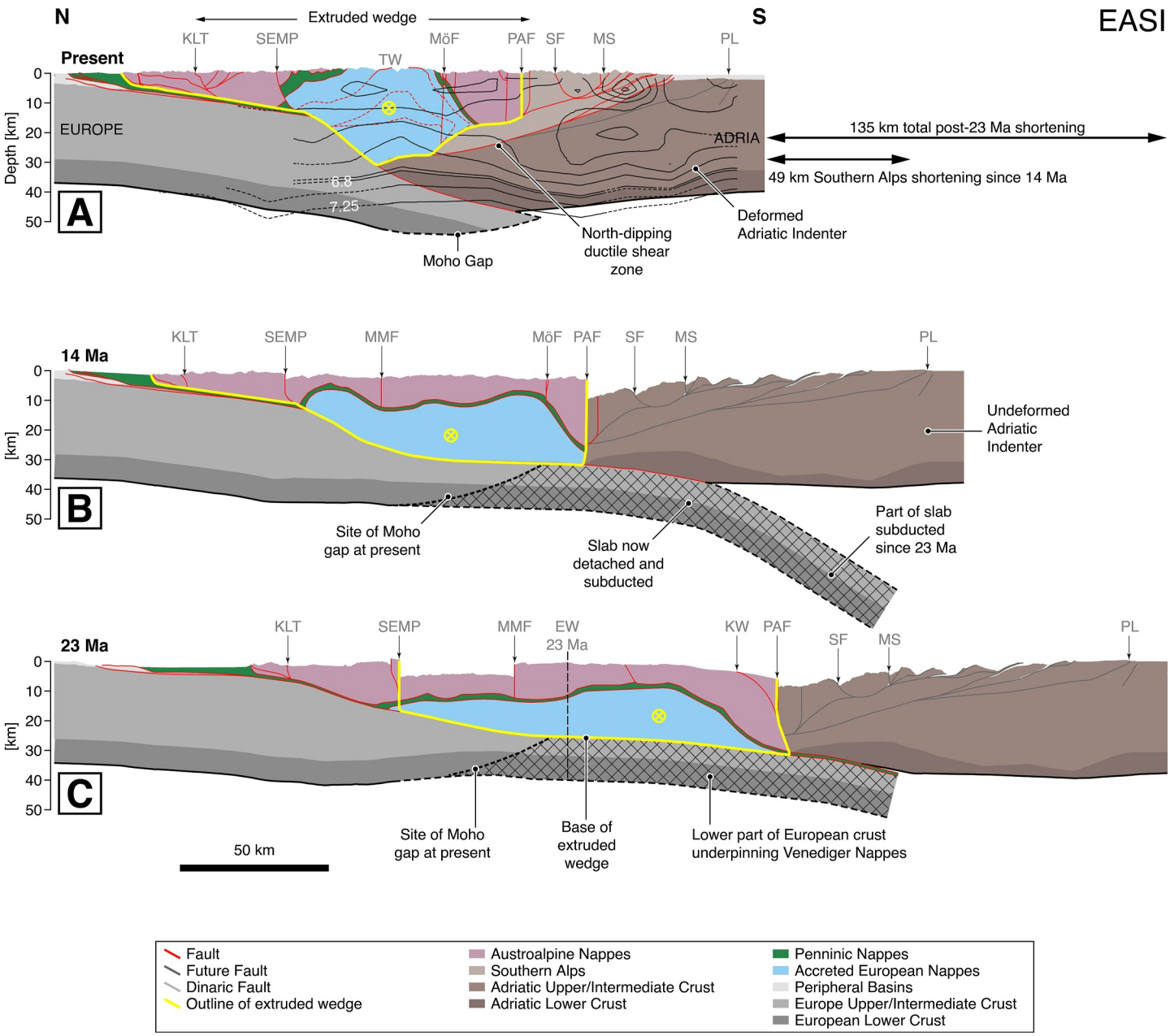

Figure 9. Restoration of the EASI cross-section from Present (a) back to 14 Ma (b) and 23 Ma (c). Faults bounding the eastwardly extruding wedge are highlighted in yellow. LET P-wave velocity contours at intervals of 0.25 km/s in (a) are taken from Jozi Najafabadi et al. (2022). Tectonic units labeled 1–6 aid in the description of the retrodeformation in the text. The slab end in (a) is interpreted from P-wave teleseismic tomography, the location of the Moho gap, and LET P-wave velocity contours in Figure 7A. The cross-hatched gray area represents the European crust south of the present-day down-dip end of the positive velocity anomaly of the European slab. This end in panels (b, c) corresponds to the location of the Moho gap marked in panel (a), see text for discussion.

the hangingwall of the lower crustal wedge, which is imaged as a high-velocity anomaly in subsurface seismic images (Figures 3c and 9a).

In both the 14 and 23 Ma cross-sections (Figures 9b and 9c), we account for orogen-parallel transport using laterally offset cross-sections (Figure 4). Eastward orogen-parallel transport accommodated a total of 43 km of N-S shortening since 23 Ma, with 31 km of this N-S shortening accommodated from 23 to 14 Ma and an additional 12 km from 14 Ma to the present.

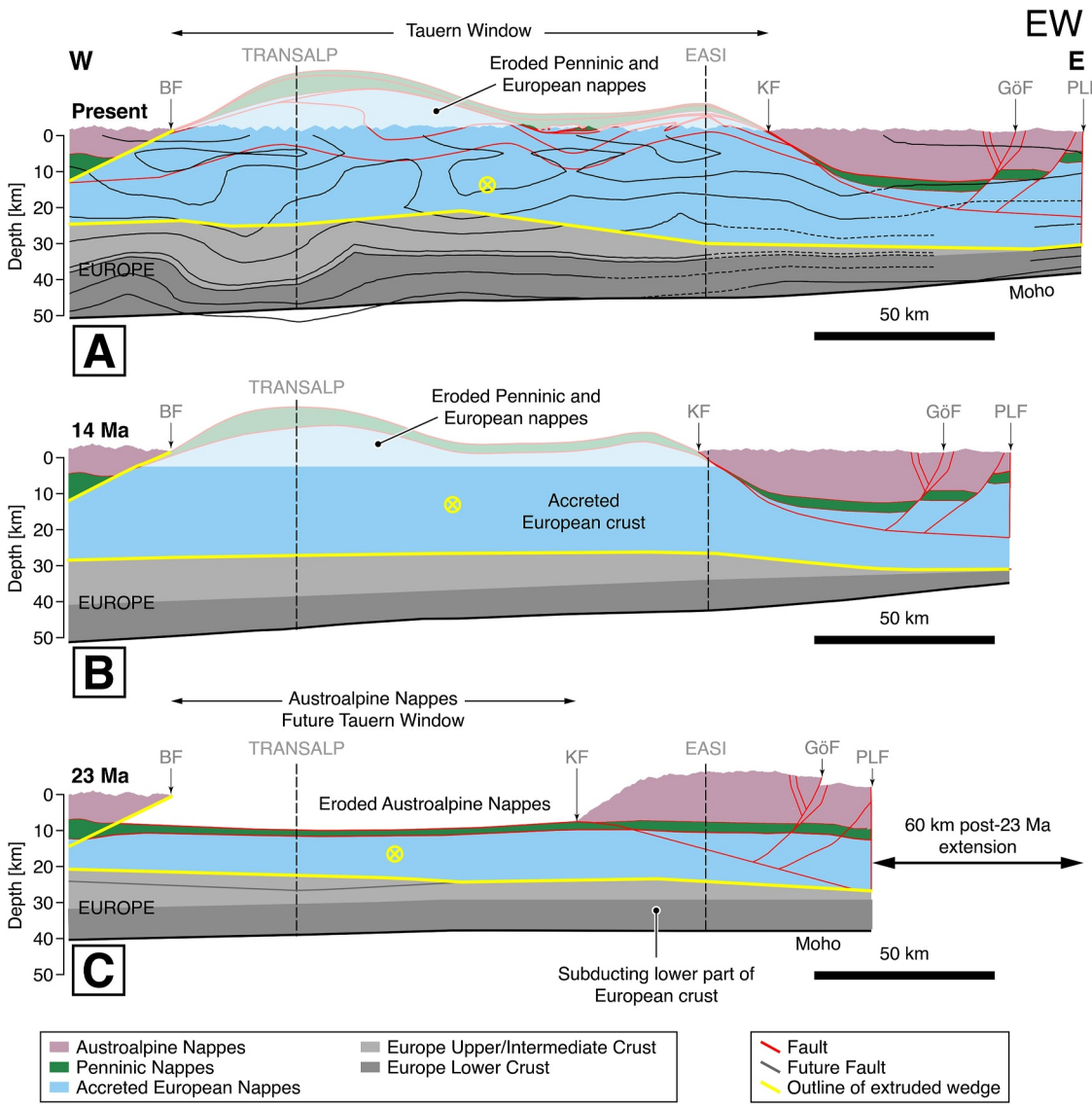

Figure 10. Restoration of the EW cross-section from Present (a) to 14 Ma (b), 23 Ma (b). Faults bounding the eastwardly extruding wedge are highlighted in yellow. LET contours at intervals of 0.25 km/s in panel (a) are taken from Jozi Najafabadi et al. (2022). BF—Brenner Fault; GöF—Görschitztal Fault; KF—Katschberg Fault; PLF—Pöls-Lavanttal Fault.

From the 14 Ma to the 23 Ma reconstruction in Figure 9c, we restore ~20 km shortening due to out-of-sequence thrusting below the Northern Calcareous Alps. This is required to accommodate shortening between 20 and 9 Ma associated with NE-translation of the Northern Calcareous Alps along the oblique-sinistral Inntal Fault once northward propagation of Subalpine Molasse thrusting had ceased (~20 Ma; Hinsch, 2013). Most of this out-of-sequence thrusting occurred within the Penninic and Helvetic nappes and by thrusting of the Northern Calcareous Alps over these nappes (Beidinger & Decker, 2014; Hinsch, 2013). Using the ~20 km estimate of out-of-sequence shortening, we restore the Penninic and Helvetic nappes as a single unit, preserving cross-sectional area. Poor surface exposure and a lack of internal reflectors in the seismic data presented in Hinsch (2013) make subsurface interpretation highly uncertain. As in the TRANSALP cross-section, we extend the European lower crust below the unfolded Venediger Nappes.

6.3. EW (Orogen-Parallel)

To restore the present EASI cross-section in Figure 10a to 23 Ma (Figure 10c), we first translate the cross-section line (Figure 2) southward to account for shortening by upright folding exposed in the Tauern Window (see

Figures 8c and 9c for intersection of the EW cross-section with the TRANSALP and EASI cross-sections at 23 Ma). The thickness of the Venediger Nappes and subducting European crust is estimated by using the intersections with TRANSALP and EASI cross-sections (Figures 8c and 9c). We then restore at total of 60 km of extension reported on the Brenner and Katschberg faults (Fügenschuh et al., 2012; Scharf et al., 2013; Wolff et al., 2021).

7. Behavior of Orogenic Lithosphere During Indentation

7.1. Timing of Indentation and the Mechanical Response of the Indented Crust

Indentation of the Eastern Alps occurred in two phases, first involving the whole Adriatic crust from ~23 to 14 Ma, then followed by N-S shortening of the leading edge of the Adriatic Plate since 14 Ma. The first phase of indentation coincided with the cessation of the northward advance of the thrust front into the Molasse Basin, north of Salzburg (Figure 2; Hinsch, 2013; Ortner et al., 2014). The Adriatic indenter moved north along the northern segment of the Giudicarie Fault, displacing the Periadriatic Fault by some 70 km (e.g., Laubscher, 1990; Schönborn, 1992). This motion was largely accommodated by post-nappe, upright folding in the Tauern Window. The second phase entailed wedging of the Adriatic middle and lower crust into the base of the Eastern Alpine orogenic wedge.

Upright folding in the Tauern Window was broadly coeval with E-W extension on the Katschberg and Brenner faults, as argued on structural and thermochronological grounds (Fügenschuh et al., 1997; Rosenberg et al., 2018; Scharf et al., 2013). This was linked to eastward extrusion of the high-grade metamorphic core of the Eastern Alps between conjugate, oblique strike-slip faults (Figure 2). In the TRANSALP and EASI cross-sections for 23 Ma (Figures 8c and 9c), we infer that these faults flatten into a common detachment surface (*sensu* Oldow et al., 1990) at the base of the Venediger Nappes at ~25 km depth as highlighted in yellow in Figures 8–10. Above this basal detachment, we restore 67 and 42 km of shortening in the TRANSALP and EASI cross-sections, respectively. Going from west to east along the Tauern Window, the proportion of N-S shortening accommodated by upright folding decreases and the proportion of shortening by orogen-parallel transport increases. Rosenberg et al. (2018, their Figure 23) schematically illustrated how a series of easterly diverging conjugate strike-slip faults account for these trends. In the western Tauern Window, orogen-parallel transport was accommodated primarily by the Inntal and Periadriatic faults. In the eastern Tauern Window, the SEMP, ZWD, and Mölltal Faults accommodated additional orogen-parallel transport (Figure 4), leading to an eastward increase in orogen-parallel displacement relative to the European foreland and thus an eastward increase in shortening taken up by orogen parallel motion. A consequence of placing the basal detachment at the base of the Venediger Nappes (Figures 8–10) is that shortening in the east was accommodated without significant crustal thickening, whereas in the west, south-directed subduction of the European lithosphere accommodated N-S convergence of the underlying lower crust and mantle lithosphere.

The Venediger Nappes were affected by Barrow-type metamorphism between 32 and 25 Ma, resulting in temperatures of 500–600°C (e.g., Favaro et al., 2017; Schuster et al., 2004). Given the strong temperature sensitivity of crustal viscosity (e.g., Carter & Tsenn, 1987; Handy, 1989; Kohlstedt et al., 1995), high temperatures are expected to have reduced the viscous strength of the nappe pile in the Tauern Window during burial in Paleogene time. During subsequent indentation, upright isoclinal folding rotated the main foliation into increasingly high angles with the direction of indentation, thus increasing the bulk viscous strength of the Venediger Nappes in the N-S direction of indentation, an effect known in rock mechanics as geometric- or foliation-hardening. The nappes are expected to have strengthened even more as they exhumed and cooled below 300°C, that is, through the viscous-to-frictional transition in granitoid rocks (e.g., Handy et al., 1999). Strengthening rendered the nappe stack a strong body that resisted further indentation, such that N-S convergence was increasingly accommodated by south-directed folding and thrusting, forming the eastern Southern Alps.

7.2. Crustal Wedging

During the second phase of indentation, a ductile shear zone in the Southern Alps basement accommodated northward wedging of the Adriatic middle-to-lower crust above subducted European lithosphere in the TRANSALP and EASI cross-sections (Figures 8 and 9). This wedging is kinematically like the wedging proposed for the NFP-20E cross-section west of the Giudicarie Fault (e.g., Schmid et al., 1996, and references therein, see also Rosenberg & Kissling, 2013). In contrast to the NFP-20E cross-section, however, the indented orogenic

wedge east of the Giudicarie Fault comprises both accreted European and Adriatic units. The latter were emplaced as nappes during late Cretaceous and Paleogene accretion and subduction (Schmid et al., 2004; Schuster et al., 2004), that is, prior to Neogene indentation.

The model of crustal indentation and European subduction in Figures 6a and 6b differs markedly from past interpretations in which the middle to lower crust of the eastern Southern Alps was subducted on a north-dipping slab of Adriatic lithosphere (e.g., Handy et al., 2015; Lippitsch, 2002; Schmid et al., 2004). Here, we follow Mitterbauer et al. (2011) in interpreting the positive P-wave velocity anomaly beneath the Eastern Alps as a remnant of the subducted European Plate. Handy et al. (2021) argued against an Adriatic origin for this slab because its 100–200 km down-dip length far exceeds shortening in the Southern Alps (Figures 8 and 9; Castellarin et al., 1998).

North of the Periadriatic Fault, we find around 90 km total shortening (92 km in TRANSALP, Figure 8; 86 km in EASI, Figure 9). This shortening, involving European-accreted nappes, occurred above the European lithosphere (Figures 6a and 6b and 8 and 9), requiring subduction equivalent to the shortening we reconstruct. Along the TRANSALP cross-section, the slab corresponding to this shortening is imaged as a south-dipping positive velocity anomaly in teleseismic P-wave tomography (Figure 7a). European subduction must have been continuous but slow throughout the Neogene to accommodate Adriatic indentation that involved upright folding, orogen-parallel extrusion, and orogen-normal thrusting.

7.3. Constraints on Subduction and Possible Slab Removal Events

The approximate age of the positive velocity anomalies that are interpreted as subducted slabs can be constrained by comparing the current slab lengths in Figure 7 with the amount of N-S shortening estimated from the three-dimensionally balanced cross-sections in Figures 8 and 9. In so doing, we assume that lithospheric volume is conserved during subduction. Crustal shortening estimates obtained by retrodeforming nappe systems must always be regarded as minima in the absence of both adequate cutoff markers and evidence precluding subduction erosion. Also, slab lengths are difficult to measure and compare in teleseismic tomographic images, not only due to poor resolution and smearing of the images (e.g., Foulger et al., 2013), but also because slabs themselves may be deformed (Lister et al., 2008). In the model used here (Paffrath et al., 2021), the reported vertical resolution is about 20 km down to ∼150 km depth and decreases to 50 km at greater depth, with considerable smearing at depths down to ∼350 km, the maximum depth considered here. Despite these limitations, the combined geological-geophysical approach below yields general insight into the possible volumes and ages of subducted lithosphere beneath the Eastern Alps.

The south-dipping slab anomaly in the TRANSALP cross-section (Figure 7a) is at least 200 km long, exceeding the 138 km of post-23 Ma N-S shortening estimated above along this cross-section (Figure 8). Some of this difference may be attributed to stretching of the down-going slab under its own weight (e.g., Lister et al., 2008), but the estimates are similar enough to indicate that the slab still attached to the orogenic lithosphere represents lithosphere mostly subducted since 23 Ma. The down-dip end of this anomaly may therefore represent a slab detachment surface at about 23 Ma. Extensive analysis of tomographic slices in this area indicates that this high-velocity anomaly actually connects out-of-section with the vertically underlying positive anomaly at 220–350 km depth. This is inferred to comprise lithosphere that subducted mostly before 23 Ma, that is, in Paleogene time (Figure 7a).

In contrast, the EASI cross-section lacks a slab anomaly and instead features only a thin high velocity layer beneath the Moho (Figure 7b). Thus, there is no slab still attached to the orogenic lithosphere to accommodate the total of 135 km of N-S shortening in this cross-section since 23 Ma (Figures 9b and 9c). The only plausible candidate for this slab is the positive anomaly in Figures 7b and 7c entrained between 150 and 300 km depth. In the EASI cross-section, the ∼150 km down-dip length of this anomaly exceeds post-23 Ma shortening by only 15 km. Taken at face value, the excess length of the anomaly indicates either that the slab underwent down-dip stretching and/or that it includes some 15 km of European lithosphere that was subducted before 23 Ma. Thus, like the TRANSALP cross-section, the bottom of the anomaly in the EASI cross-section may lie at or near a slab detachment surface at 23 Ma.

The western part of this large anomaly, which is the same positive anomaly imaged between 220 and 350 km depth in the TRANSALP cross-section (Figure 7a), is inferred to comprise older lithosphere subducted prior to

23 Ma based on the arguments above. Thus, by applying areal balancing of crustal shortening, we surmise that what appears as a single large positive anomaly in Figure 7c is actually a segmented slab. Lines delineating older and younger segments are drawn accordingly in Figure 7c. The resolution of the P-wave tomographic model used here (Paffrath et al., 2021) is insufficient to distinguish closely spaced slab segments at this depth.

Shallow removal of the slab in EASI cross-section must have occurred after 23 Ma, possibly even after 14 Ma to account for the lack of slab to accommodate the 68 km of post-14 Ma N-S shortening estimated above (Figures 9a and 9b). Shallow slab removal earlier than 14 Ma can be ruled out because asthenosphere would have been emplaced in direct contact with the base of the Venediger Nappes (cross-hatched area in Figures 9b and 9c). This is implausible in the absence of mid-Miocene metamorphism and volcanism in the Eastern Alps (e.g., Göğüş & Pysklywec, 2008; Reid et al., 2017). Therefore, we propose that the European lithosphere in the upper part of the detached slab in the EASI cross-section formed the substratum of the Venediger Nappes beneath the Sub-Tauern Ramp until it detached, sometime after 14 Ma.

In keeping with this scenario, we interpret the thin high-velocity anomaly beneath the EASI cross-section to be newly formed mantle lithosphere (marked new LAB in Figures 7b and 7c) that has grown since the last slab removal event at ≤14 Ma. The negative velocity anomaly in P-wave tomography in the depth interval of 70–150 km of the EASI cross-section (Figures 7b and 7c) is thought to represent asthenosphere filling the sub-horizontal gap left by this slab removal. Notably, this negative velocity anomaly does not extend as far west as the TRANSALP cross-section. It neither coincides with the northern projection of the Giudicarie Fault (Figures 2 and 7c), nor does it line up with the eastern and western ends of the Tauern Window. This discrepancy in the location of crustal and mantle structures suggests that the major faults exposed at the surface formed before slab removal at ≤14 Ma as argued below.

7.4. Geological Expression of Slab Removal Events

What was the geological expression of the slab removal events inferred above from tectonic balancing and P-wave seismic tomography? Partial detachment of subducting European lithosphere in early Miocene time fits well with previous proposals of slab detachment (Handy et al., 2015, 2021; Schlunegger & Kissling, 2022) to explain sudden tectonic uplift and coeval infilling of the marine eastern Molasse Basin in Burdigalian time (e.g., Hülscher et al., 2019; Kuhlemann & Kempf, 2002; Le Breton et al., 2023). This uplift may represent the terminal stages of slab detachment that began at ∼23 Ma, facilitating the indentation and orogen-parallel extension of the Eastern Alps, as well as triggering extension in the Pannonian Basin in the upper plate of the retreating Carpathian subduction orogen. It may also have initiated the mid-Miocene change in orogenic polarity from N-directed thrusting along the northern front of the eastern Alps to S-directed folding and thrusting in the Southern Alps. These events immediately predated and were continuous with the ∼20 Ma onset of major east-west extension in the Pannonian Basin that accompanied roll-back subduction in the Carpathians (∼200–300 km; e.g., Horváth et al., 2006, 2015; Royden & Burchfiel, 1989; Ustaszewski et al., 2008). Thus, Adriatic indentation rather than Carpathian roll-back subduction was the probable trigger of orogen-parallel extension in the Eastern Alps (Scharf et al., 2013; Schmid et al., 2013).

Evidence for removal of part of the European slab beneath the Eastern Alps after 14 Ma is more difficult to find in the geologic record. The eastern Molasse Basin underwent 500–900 m of post-Late Miocene erosion (Gusterhuber et al., 2012) that has been tied to 200–600 m of Late Mio-Pliocene tectonic uplift (Genser et al., 2007). Within the Eastern Alps, the Tauern Window saw high exhumation rates in Mio-Pliocene times, based on inversion of thermochronological data (∼700 m/Myr, e.g., Bertrand et al., 2017; Fox et al., 2015; Heberer et al., 2017). Mio-Pliocene uplift was also active east of the Tauern Window based on dating of incised high-elevation low-relief surfaces (Gradwohl et al., 2024; Stüwe et al., 2024), catchment-wide erosion-rate modeling (Legrain et al., 2014) and dating of sediments in cave systems (Wagner et al., 2010).

A possible explanation for these ≤14 Ma events is that low subduction rates in the Miocene (3–4 mm/yr average based on our shortening estimates) allowed the slab to steepen and heat up as Adria-Europe convergence ground to a halt. Pull of the residual slab may have thinned the slab, promoting thermal erosion and decreasing the viscosity of the slab, thus rendering it more deformable while gradually increasing its buoyancy and decreasing its downward pull. Taken together, these factors would be expected to locally increase the rates and amounts of surface response. However, such effects are speculative and difficult, if not impossible, to distinguish at the surface.

Finally, we note that Neogene slab detachment(s) does not preclude an older slab detachment event in Eo-Oligocene time, which has long been proposed to explain calc-alkaline magmatism along the Periadriatic Fault (von Blanckenburg & Davies, 1995) and rapid uplift and erosion of the retro-wedge of the Central Alps (e.g., Schlunegger & Castelltort, 2016; Sinclair, 1997). Thus, the Eastern Alps may well have witnessed up to three late-to post-collisional slab removal events, resulting in the complex three-dimensional slab geometries imaged today by P-wave tomography in the AlpArray experiment.

8. Conclusions

We have reconstructed the Neogene to Present structural evolution of the Eastern Alps in N-S (TRANSALP and EASI) and E-W (orogen-parallel) cross-sections of the orogenic wedge that are corrected for out-of-section orogen-parallel transport. Correlating these three-dimensionally balanced cross-sections with the geological record reveals two phases of Adriatic indentation of the Eastern Alpine orogenic wedge. During these phases, the total N-S shortening of ∼135 km north of the Periadriatic Fault in both the TRANSALP and EASI transects was accommodated by a roughly equivalent amount of subduction of European lithosphere.

The first phase of indentation (∼23–14 Ma), concurrent with the termination of northward thrust advancement into the Molasse Basin, involved the northward movement of the Dolomites sub-indenter of the Adriatic Plate along the Giudicarie Fault. This movement displaced the Periadriatic Fault by some 70 km and was accompanied by post-nappe upright folding, and E-W extension in the Tauern Window. The latter was broadly coeval with eastward orogen-parallel transport (Rosenberg et al., 2018; Scharf et al., 2013; Wölfler et al., 2011) at an average rate of ≥4 mm/yr. We propose that this first phase of indentation was triggered by detachment of the European slab beneath large parts of the Eastern Alps, beginning at 23 Ma.

The second phase of indentation (∼14–0 Ma) involved deformation of the leading edge of the Adriatic indenter, forming the Southern Alps fold-thrust belt as the Adriatic middle-to-lower crust wedged into the base of the Eastern Alpine orogenic wedge. We tentatively relate this second phase of indentation to gradual removal of the part of the European slab remaining after the earlier detachment event. There is no unequivocal surface expression of this late slab removal, possibly indicating a slab load that had already been reduced by earlier slab detachment(s).

In parting, we note that our exploration of the consequences of slab detachment on the orogenic crust involved using only the P-wave tomographic model of Paffrath et al. (2021), Yet, in the Alps, differences remain among seismological models based on different methods and among models using the same method (Kästle et al., 2020). These differences are most pronounced in the crucial depth interval between 70 and 150 km (Paffrath et al., 2021). This underscores the need for rigorous benchmarking of seismological models (e.g., Kästle & Paffrath, 2023), which may help us to ascertain whether tomographic images portray a physical reality or merely reflect the myriad assumptions made in collecting, processing, and inverting seismic waveforms. Using geological data on the age and kinematics of crustal motion provides an independent means of testing the viability of seismological models.

Acknowledgments
We acknowledge the support of the German Science Foundation (DFG) in the form of research Grant Ha 2403/23-2 to the second author. This grant supported the first author and all coordination activities of the research priority program SPP-2017 entitled "Mountain Building in 4-Dimensions (4D-MB)." We are grateful to Kurt Stüwe and Franz Neubauer for their constructive reviews. Our sincere thanks also go to many colleagues in 4D-MB, amongst them those who took the time to discuss, but do not necessarily agree with, the conclusions reached here: Eline Le Breton, Marcel Paffrath, Stefan Schmid, Emanuel Kästle, Christian Haberland, Azam Jozi Najafabadi, Klaus Bauer. We thank PE Ltd for donating academic licences for *Move*™ structural modeling and analysis software. Open Access funding enabled and organized by Projekt DEAL.

Data Availability Statement

Local earthquake tomography data are available in Jozi Najafabadi et al. (2022). P-wave teleseismic tomography data can be accessed in Paffrath et al. (2021). Reflection seismic data are available through Lüschen et al. (2006). Geological maps used in cross-section construction are listed in Supporting Information S1.

References

AlpArray Seismic Network Team, AlpArray OBS Cruise Crew, Working Group, Hetényi, G., Molinari, I., Clinton, J., Bokelmann, G., et al. (2018). The AlpArray seismic network: A large-scale European experiment to image the Alpine Orogen. *Surveys in Geophysics*, *39*(5), 1009–1033. https://doi.org/10.1007/s10712-018-9472-4

Anderlini, L., Serpelloni, E., Tolomei, C., De Martini, P. M., Pezzo, G., Gualandi, A., & Spada, G. (2020). New insights into active tectonics and seismogenic potential of the Italian Southern Alps from vertical geodetic velocities. *Solid Earth*, *11*(5), 1681–1698. https://doi.org/10.5194/se-11-1681-2020

Auer, M., & Eisbacher, G. H. (2003). Deep structure and kinematics of the northern Calcareous Alps (TRANSALP profile). *International Journal of Earth Sciences*, *92*(2), 210–227. https://doi.org/10.1007/s00531-003-0316-0

Bartel, E. M., Neubauer, F., Heberer, B., & Genser, J. (2014). A low-temperature ductile shear zone: The gypsum-dominated western extension of the brittle Fella-Sava Fault, Southern Alps. *Journal of Structural Geology*, *69*, 18–31. https://doi.org/10.1016/j.jsg.2014.09.016

Bartosch, T., Stüwe, K., & Robl, J. (2017). Topographic evolution of the Eastern Alps: The influence of strike-slip faulting activity. *Lithosphere*, *9*(3), 384–398. https://doi.org/10.1130/L594.1

Battista Carulli, G., Della Vedova, B., Podda, F., Slejko, D., & Zanolla, C. (2006). Carta Geologica del Friuli Venezia Giulia [Map]. *Servizio Geologico Regione Autonoma Friuli Venezia Giulia*.

Bauer, K., Schwarz, B., Trichandi, R., Wawerzinek, B., McPhee, P., & Handy, M. R. (2024). New insights into seismic structures around the Tauern Window and the Periadriatic Fault System from reprocessing of TRANSALP seismic reflection data. https://doi.org/10.5194/egusphere-egu24-11066

Beidinger, A., & Decker, K. (2014). Quantifying early Miocene in-sequence and out-of-sequence thrusting at the Alpine-Carpathian junction: Reconstruction of thrusting eastern Alps. *Tectonics*, *33*(3), 222–252. https://doi.org/10.1002/2012TC003250

Bertotti, G., Siletto, G. B., & Spalla, M. I. (1993). Deformation and metamorphism associated with crustal rifting: The Permian to Liassic evolution of the lake Lugano-Lake Como area (southern Alps). *Tectonophysics*, *226*(1), 271–284. https://doi.org/10.1016/0040-1951(93)90122-Z

Bertrand, A., Rosenberg, C., Rabaute, A., Herman, F., & Fügenschuh, B. (2017). Exhumation mechanisms of the Tauern Window (Eastern Alps) inferred from apatite and zircon fission track thermochronology: Exhumation of the Tauern window. *Tectonics*, *36*(2), 207–228. https://doi.org/10.1002/2016TC004133

Bianchi, I., Ruigrok, E., Obermann, A., & Kissling, E. (2021). Moho topography beneath the European Eastern Alps by global-phase seismic interferometry. *Solid Earth*, *12*(5), 1185–1196. https://doi.org/10.5194/se-12-1185-2021

Bijwaard, H., & Spakman, W. (2000). Non-linear global *P* -wave tomography by iterated linearized inversion. *Geophysical Journal International*, *141*(1), 71–82. https://doi.org/10.1046/j.1365-246X.2000.00053.x

Bleibinhaus, F., & Groschup, R. (2008). Structure of the Periadriatic Fault in the eastern Alps from reflection seismic imaging. American Geophysical Union, Fall Meeting 2008, San Francisco.

Brack, P. (1981). Structures in the southwestern border of the Adamello intrusion (Alpi Bresciane, Italy). *Schweizerische Mineralogische Und Petrographische Mitteilungen*, *61*(1), 37–49. https://doi.org/10.5169/seals-47129

Bressan, G., Ponton, M., Rossi, G., & Urban, S. (2016). Spatial organization of seismicity and fracture pattern in NE Italy and W Slovenia. *Journal of Seismology*, *20*(2), 511–534. https://doi.org/10.1007/s10950-015-9541-9

Brix, F., & Schultz, O. (1993). *Erdöl und Erdgas in Österreich* (2nd ed.). Naturhistorisches Museum Wien. Retrieved from https://opac.geologie.ac.at/ais312/detail.aspx

Buiter, S. J. H., Govers, R., & Wortel, M. J. R. (2002). Two-dimensional simulations of surface deformation caused by slab detachment. *Tectonophysics*, *354*(3–4), 195–210. https://doi.org/10.1016/S0040-1951(02)00336-0

Burke, M. M., & Fountain, D. M. (1990). Seismic properties of rocks from an exposure of extended continental crust—New laboratory measurements from the Ivrea zone. *The Nature of the Lower Continental Crust*, *182*(1), 119–146. https://doi.org/10.1016/0040-1951(90)90346-A

Carter, N. L., & Tsenn, M. C. (1987). Flow properties of continental lithosphere. *Tectonophysics*, *136*(1–2), 27–63. https://doi.org/10.1016/0040-1951(87)90333-7

Castellarin, A., & Cantelli, L. (2000). Neo-alpine evolution of the southern eastern Alps. *Journal of Geodynamics*, *30*(1–2), 251–274. https://doi.org/10.1016/S0264-3707(99)00036-8

Castellarin, A., Cantelli, L., Fesce, A. M., Mercier, J. L., Picotti, V., Pini, G. A., et al. (1992). Alpine compressional tectonics in the southern Alps. Relationships with the N-Apennines. *Annales Tectonicae*, *4*(1), 62–94.

Castellarin, A., Luigi, S., Picotti, V., & Cantelli, L. (1998). La tettonica delle Dolomiti nel quadro delle Alpi Meridionali Orientali. *Mem. Soc. Geol. Ital.*, *53*, 133–143.

Castellarin, A., Nicolich, R., Fantoni, R., Cantelli, L., Sella, M., & Selli, L. (2006). Structure of the lithosphere beneath the Eastern Alps (southern sector of the TRANSALP transect). *24*.

Castellarin, A., Vai, G. B., & Cantelli, L. (2006). The Alpine evolution of the southern Alps around the Giudicarie faults: A late Cretaceous to early Eocene transfer zone. *Tectonophysics*, *414*(1–4), 203–223. https://doi.org/10.1016/j.tecto.2005.10.019

Diehl, T., Husen, S., Kissling, E., & Deichmann, N. (2009). High-resolution 3-D *P* -wave model of the Alpine crust. *Geophysical Journal International*, *179*(2), 1133–1147. https://doi.org/10.1111/j.1365-246X.2009.04331.x

Doglioni, C., & Bosellini, A. (1987). Eoalpine and mesoalpine tectonics in the southern Alps. *Geologische Rundschau*, *76*(3), 735–754. https://doi.org/10.1007/BF01821061

Duretz, T., Gerya, T. V., & May, D. A. (2011). Numerical modelling of spontaneous slab breakoff and subsequent topographic response. *Tectonophysics*, *502*(1–2), 244–256. https://doi.org/10.1016/j.tecto.2010.05.024

Eder, N., & Neubauer, F. (2000). On the edge of the extruding wedge: Neogene kinematics and geomorphology along the southern Niedere Tauern, Eastern Alps. *Eclogae Geologicae Helvetiae*, *93*, 81–92.

Eizenhöfer, P. R., Glotzbach, C., Kley, J., & Ehlers, T. A. (2023). Thermo-kinematic evolution of the eastern European Alps along the TRANSALP transect. *Tectonics*, *42*(4), e2022TC007380. https://doi.org/10.1029/2022TC007380

Elias, J. (1998). The thermal history of the Ötztal Stubai complex (Tyrol, Austria, Italy) in the light of the lateral extrusion model. Inst. und Museum für Geologie und Paläontologie Tübingen; WorldCat.

Favaro, S., Handy, M. R., Scharf, A., & Schuster, R. (2017). Changing patterns of exhumation and denudation in front of an advancing crustal indenter, Tauern window (eastern Alps): Indentation, exhumation and Denudation. *Tectonics*, *36*(6), 1053–1071. https://doi.org/10.1002/2016TC004448

Favaro, S., Schuster, R., Handy, M. R., Scharf, A., & Pestal, G. (2015). Transition from orogen-perpendicular to orogen-parallel exhumation and cooling during crustal indentation—Key constraints from 147Sm/144Nd and 87Rb/87Sr geochronology (Tauern window, Alps). *Tectonophysics*, *665*, 1–16. https://doi.org/10.1016/j.tecto.2015.08.037

Fodor, L., Jelen, B., Márton, E., Skaberne, D., Čar, J., & Vrabec, M. (1998). Miocene-Pliocene tectonic evolution of the Slovenian Periadriatic fault: Implications for Alpine-Carpathian extrusion models. *Tectonics*, *17*(5), 690–709. https://doi.org/10.1029/98TC01605

Foulger, G. R., Panza, G. F., Artemieva, I. M., Bastow, I. D., Cammarano, F., Evans, J. R., et al. (2013). Caveats on tomographic images. *Terra Nova*, *25*(4), 259–281. https://doi.org/10.1111/ter.12041

Fox, M., Herman, F., Kissling, E., & Willett, S. D. (2015). Rapid exhumation in the Western Alps driven by slab detachment and glacial erosion. *Geology*, *43*(5), 379–382. https://doi.org/10.1130/G36411.1

Frisch, W., Dunkl, I., & Kuhlemann, J. (2000). Post-collisional orogen-parallel large-scale extension in the Eastern Alps. *Tectonophysics*, *327*(3–4), 239–265. https://doi.org/10.1016/S0040-1951(00)00204-3

Frisch, W., & Gawlick, H.-J. (2003). The nappe structure of the central northern Calcareous Alps and its disintegration during Miocene tectonic extrusion—A contribution to understanding the orogenic evolution of the eastern Alps. *International Journal of Earth Sciences*, *1*(1), 1. https://doi.org/10.1007/s00531-003-0357-4

Fügenschuh, B. (1995). Thermal and kinematic history of the Brenner area (eastern Alps, Tyrol). *ETH Zurich*.
Fügenschuh, B., Mancktelow, N. S., & Schmid, S. S. (2012). Comment on Rosenberg and Garcia: Estimating displacement along the Brenner Fault and orogen-parallel extension in the eastern Alps. *International Journal of Earth Sciences*, *101*(5), 1451–1455. https://doi.org/10.1007/s00531-011-0725-4
Fügenschuh, B., Seward, D., & Mancktelow, N. (1997). Exhumation in a convergent orogen: The western Tauern window. *Terra Nova*, *9*(5–6), 213–217. https://doi.org/10.1111/j.1365-3121.1997.tb00015.x
Garzanti, E., Radeff, G., & Malusà, M. G. (2018). Slab breakoff: A critical appraisal of a geological theory as applied in space and time. *Earth-Science Reviews*, *177*, 303–319. https://doi.org/10.1016/j.earscirev.2017.11.012
Genser, J., Cloetingh, S. A. P. L., & Neubauer, F. (2007). Late orogenic rebound and oblique Alpine convergence: New constraints from subsidence analysis of the Austrian Molasse basin. *Global and Planetary Change*, *58*(1–4), 214–223. https://doi.org/10.1016/j.gloplacha.2007.03.010
Göğüş, O. H., & Pysklywec, R. N. (2008). Mantle lithosphere delamination driving plateau uplift and synconvergent extension in eastern Anatolia. *Geology*, *36*(9), 723. https://doi.org/10.1130/G24982A.1
Gradwohl, G., Stüwe, K., Liebl, M., Robl, J., Plan, L., & Rummler, L. (2024). The elevated low-relief landscapes of the Eastern Alps. *Geomorphology*, *458*, 109264. https://doi.org/10.1016/j.geomorph.2024.109264
Groß, P., Handy, M. R., John, T., Pestal, G., & Pleuger, J. (2020). Crustal-scale Sheath folding at HP conditions in an exhumed Alpine subduction zone (Tauern window, eastern Alps). *Tectonics*, *39*(2), e2019TC005942. https://doi.org/10.1029/2019TC005942
Groß, P., Pleuger, J., & Handy, M. R. (2022). Rift-Related paleogeography of the European margin in the eastern Alps (central Tauern window). *Swiss Journal of Geosciences*, *115*(1), 27. https://doi.org/10.1186/s00015-022-00426-9
Gusterhuber, J., Dunkl, I., Hinsch, R., Linzer, H.-G., & Sachsenhofer, R. (2012). Neogene uplift and erosion in the Alpine foreland basin (upper Austria and Salzburg). *Geologica Carpathica*, *63*(4), 295–305. https://doi.org/10.2478/v10096-012-0023-5
Handy, M. R. (1989). Deformation regimes and the rheological evolution of fault zones in the lithosphere: The effects of pressure, temperature, grainsize and time. *Tectonophysics*, *163*(1–2), 119–152. https://doi.org/10.1016/0040-1951(89)90122-4
Handy, M. R., Babist, J., Wagner, R., Rosenberg, C., & Konrad, M. (2005). Decoupling and its relation to strain partitioning in continental lithosphere: Insight from the Periadriatic fault system (European Alps). *Geological Society, London, Special Publications*, *243*(1), 249–276. https://doi.org/10.1144/GSL.SP.2005.243.01.17
Handy, M. R., Franz, L., Heller, F., Janott, B., & Zurbriggen, R. (1999). Multistage accretion and exhumation of the continental crust (Ivrea crustal section, Italy and Switzerland). *Tectonics*, *18*(6), 1154–1177. https://doi.org/10.1029/1999TC900034
Handy, M. R., Giese, J., Schmid, S. M., Pleuger, J., Spakman, W., Onuzi, K., & Ustaszewski, K. (2019). Coupled crust-mantle response to slab tearing, bending, and rollback along the Dinaride-Hellenide orogen. *Tectonics*, *38*(8), 2803–2828. https://doi.org/10.1029/2019TC005524
Handy, M. R., McPhee, P. J., & Le Breton, E. (2023). A new 4D model of Alpine orogenesis based on AlpArray. Abstracts of the Annual AlpArray and 4D-MB Scientific Meeting, Bad Hofgastein 2023, 2 S. https://doi.org/10.17169/REFUBIUM-41036
Handy, M. R., M. Schmid, S., Bousquet, R., Kissling, E., & Bernoulli, D. (2010). Reconciling plate-tectonic reconstructions of Alpine Tethys with the geological–geophysical record of spreading and subduction in the Alps. *Earth-Science Reviews*, *102*(3–4), 121–158. https://doi.org/10.1016/j.earscirev.2010.06.002
Handy, M. R., & Oberhänsli, R. (2004). Explanatory notes to the map: Metamorphic structure of the Alps age map of the metamorphic structure of the Alps – Tectonic interpretation and outstanding problems. *Mitteilungen Der Österreichischen Mineralogischen Gesellschaft*, *149*, 201–225.
Handy, M. R., Schmid, S. M., Paffrath, M., & Friederich, W., & the AlpArray Working Group. (2021). Orogenic lithosphere and slabs in the greater Alpine area – Interpretations based on teleseismic P-wave tomography. *Solid Earth*, *12*(11), 2633–2669. https://doi.org/10.5194/se-12-2633-2021
Handy, M. R., Ustaszewski, K., & Kissling, E. (2015). Reconstructing the Alps–Carpathians–Dinarides as a key to understanding switches in subduction polarity, slab gaps and surface motion. *International Journal of Earth Sciences*, *104*(1), 1–26. https://doi.org/10.1007/s00531-014-1060-3
Heberer, B., Reverman, R. L., Fellin, M. G., Neubauer, F., Dunkl, I., Zattin, M., et al. (2017). Postcollisional cooling history of the eastern and southern Alps and its linkage to Adria indentation. *International Journal of Earth Sciences*, *106*(5), 1557–1580. https://doi.org/10.1007/s00531-016-1367-3
Heit, B., Cristiano, L., Haberland, C., Tilmann, F., Pesaresi, D., Jia, Y., et al. (2023). The SWATH-D seismological network in the Eastern Alps. Abstracts of the Annual AlpArray and 4D-MB Scientific Meeting, Bad Hofgastein 2023. Annual AlpArray and 4D-MB Scientific Meeting, Bad Hofgastein, Austria. https://doi.org/10.17169/REFUBIUM-41105
Hetényi, G., Plomerová, J., Bianchi, I., Kampfová Exnerová, H., Bokelmann, G., Handy, M. R., & Babuška, V. (2018). From mountain summits to roots: Crustal structure of the Eastern Alps and Bohemian Massif along longitude 13.3°E. *Tectonophysics*, *744*, 239–255. https://doi.org/10.1016/j.tecto.2018.07.001
Hinsch, R. (2013). Laterally varying structure and kinematics of the Molasse fold and thrust belt of the Central Eastern Alps: Implications for exploration. *AAPG Bulletin*, *97*(10), 1805–1831. https://doi.org/10.1306/04081312129
Hoinkes, G., Koller, F., & Rantitsch, G. (1999). Alpine metamorphism of the Eastern Alps [Text/html,application/pdf,text/html]. https://doi.org/10.5169/SEALS-60203
Horváth, F., Bada, G., Szafián, P., Tari, G., Ádám, A., & Cloetingh, S. (2006). Formation and deformation of the Pannonian Basin: Constraints from observational data. *Geological Society*, *32*(1), 191–206. https://doi.org/10.1144/GSL.MEM.2006.032.01.11
Horváth, F., Musitz, B., Balázs, A., Végh, A., Uhrin, A., Nádor, A., et al. (2015). Evolution of the Pannonian basin and its geothermal resources. *Geothermics*, *53*, 328–352. https://doi.org/10.1016/j.geothermics.2014.07.009
Hülscher, J., Fischer, G., Grunert, P., Auer, G., & Bernhardt, A. (2019). Selective recording of tectonic forcings in an Oligocene/Miocene submarine channel system: Insights from new age constraints and sediment volumes from the Austrian northern Alpine foreland basin. *Frontiers in Earth Science*, *7*, 302. https://doi.org/10.3389/feart.2019.00302
Jadoul, F., & Nicora, A. (1986). Stratigrafia e Paleogeografia Ladinico-Carnica delle Alpi Carniche Orientali (Versante Nord della Val Canale, Friuli). *Riv. It. Paleont. Strat.*, *92*(2), 201–238.
Jozi Najafabadi, A., Haberland, C., Le Breton, E., Handy, M. R., Verwater, V. F., Heit, B., et al. (2022). Constraints on crustal structure in the vicinity of the adriatic indenter (European Alps) from *Vp* and *Vp*/*Vs* local earthquake tomography [Data]. *Journal of Geophysical Research: Solid Earth*, *127*(2) https://doi.org/10.1029/2021JB023160
Karousova, H., Plomerova, J., & Babuska, V. (2013). Upper-mantle structure beneath the southern Bohemian Massif and its surroundings imaged by high-resolution tomography. *Geophysical Journal International*, *194*(2), 1203–1215. https://doi.org/10.1093/gji/ggt159
Kästle, E. D., & Paffrath, M. (2023). Advances in imaging the Alpine crust and mantle. Abstracts of the Annual AlpArray and 4D-MB Scientific Meeting, Bad Hofgastein 2023, 3. https://doi.org/10.17169/REFUBIUM-41043

Kästle, E. D., Rosenberg, C., Boschi, L., Bellahsen, N., Meier, T., & El-Sharkawy, A. (2020). Slab break-offs in the Alpine subduction zone. *International Journal of Earth Sciences*, *109*(2), 587–603. https://doi.org/10.1007/s00531-020-01821-z

Kennett, B. L. N., Engdahl, E. R., & Buland, R. (1995). Constraints on seismic velocities in the Earth from traveltimes. *Geophysical Journal International*, *122*(1), 108–124. https://doi.org/10.1111/j.1365-246X.1995.tb03540.x

Klotz, T., Pomella, H., Reiser, M., Fügenschuh, B., & Zattin, M. (2019). Differential uplift on the boundary between the eastern and the southern European Alps: Thermochronologic constraints from the Brenner base Tunnel. *Terra Nova*, *31*(3), 281–294. https://doi.org/10.1111/ter.12398

Kohlstedt, D. L., Evans, B., & Mackwell, S. J. (1995). Strength of the lithosphere: Constraints imposed by laboratory experiments. *Journal of Geophysical Research*, *100*(B9), 17587–17602. https://doi.org/10.1029/95JB01460

Koulakov, I., Kaban, M. K., Tesauro, M., & Cloetingh, S. (2009). *P*—And *S* -velocity anomalies in the upper mantle beneath Europe from tomographic inversion of ISC data. *Geophysical Journal International*, *179*(1), 345–366. https://doi.org/10.1111/j.1365-246X.2009.04279.x

Kuhlemann, J., & Kempf, O. (2002). Post-eocene evolution of the north Alpine foreland basin and its response to Alpine tectonics. *Sedimentary Geology*, *152*(1–2), 45–78. https://doi.org/10.1016/S0037-0738(01)00285-8

Kummerow, J., Kind, R., Oncken, O., Giese, P., Ryberg, T., Wylegalla, K., & Scherbaum, F. (2004). A natural and controlled source seismic profile through the eastern Alps: Transalp. *Earth and Planetary Science Letters*, *225*(1–2), 115–129. https://doi.org/10.1016/j.epsl.2004.05.040

Kurz, W., Neubauer, F., & Genser, J. (1996). Kinematics of Penninic nappes (Glockner Nappe and basement-cover nappes) in the Tauern window (eastern Alps, Austria) during subduction and Penninc-Austroalpine collision [Text/html,application/pdf]. https://doi.org/10.5169/SEALS-167914

Laubscher, H. P. (1990). The problem of the deep structure of the southern Alps: 3-D material balance considerations and regional consequences. *Tectonophysics*, *176*(1–2), 103–121. https://doi.org/10.1016/0040-1951(90)90261-6

Le Breton, E., Bernhardt, A., Neumeister, R., Heismann, C., Borzi, A., Hülscher, J., et al. (2023). Early Miocene tectono-sedimentary shift in the eastern north Alpine foreland basin and its relation to changes in tectonic style in the eastern Alps. *Abstracts of the Annual AlpArray and 4D-MB Scientific Meeting, Bad Hofgastein 2023*. Annual AlpArray and 4D-MB Scientific Meeting, Bad Hofgastein, Austria. https://doi.org/10.17169/REFUBIUM-41056

Legrain, N., Dixon, J., Stüwe, K., von Blanckenburg, F., & Kubik, P. (2014). Post-Miocene landscape rejuvenation at the eastern end of the Alps. *Lithosphere*, *7*(1), 3–13. https://doi.org/10.1130/L391.1

Linzer, H.-G., Decker, K., Peresson, H., Dell'Mour, R., & Frisch, W. (2002). Balancing lateral orogenic float of the Eastern Alps. *Tectonophysics*, *354*(3–4), 211–237. https://doi.org/10.1016/S0040-1951(02)00337-2

Lippitsch, R. (2002). Lithosphere and upper mantle P-wave velocity structure beneath the Alps by high-resolution teleseismic tomography [PhD Thesis, ETH Zurich]. https://doi.org/10.3929/ETHZ-A-004484684

Lister, G., Kennett, B., Richards, S., & Forster, M. (2008). Boudinage of a stretching slablet implicated in earthquakes beneath the Hindu Kush. *Nature Geoscience*, *1*(3), 196–201. https://doi.org/10.1038/ngeo132

Liu, Y., Genser, J., Handler, R., Friedl, G., & Neubauer, F. (2001). ^{40} Ar/^{39} Ar muscovite ages from the Penninic-Austroalpine plate boundary, Eastern Alps. *Tectonics*, *20*(4), 526–547. https://doi.org/10.1029/2001TC900011

Lüschen, E., Borrini, D., Gebrande, H., Lammerer, B., Millahn, K., Neubauer, F., & Nicolich, R. (2006). TRANSALP—Deep crustal vibroseis and explosive seismic profiling in the eastern Alps. *Tectonophysics*, *414*(1–4), 9–38. https://doi.org/10.1016/j.tecto.2005.10.014

Lüschen, E., Lammerer, B., Gebrande, H., Millahn, K., & Nicolich, R. (2004). Orogenic structure of the Eastern Alps, Europe, from TRANSALP deep seismic reflection profiling [Data]. *Tectonophysics*, *388*(1–4), 85–102. https://doi.org/10.1016/j.tecto.2004.07.024

Luth, S. W., & Willingshofer, E. (2008). Mapping of the post-collisional cooling history of the Eastern Alps. *Swiss Journal of Geosciences*, *101*(S1), 207–223. https://doi.org/10.1007/s00015-008-1294-9

Malusà, M. G., Guillot, S., Zhao, L., Paul, A., Solarino, S., Dumont, T., et al. (2021). The deep structure of the Alps based on the CIFALPS seismic experiment: A synthesis. *Geochemistry, Geophysics, Geosystems*, *22*(3), e2020GC009466. https://doi.org/10.1029/2020GC009466

Mancktelow, N. S., Stöckli, D. F., Grollimund, B., Müller, W., Fügenschuh, B., Viola, G., et al. (2001). The DAV and Periadriatic fault systems in the Eastern Alps south of the Tauern window. *International Journal of Earth Sciences*, *90*(3), 593–622. https://doi.org/10.1007/s005310000190

Maros, G., Albert, G., Szeiler, R. B., Fodor, L., Gyalog, Jocha-Edelényi, E., Kercsmár, Z. S., et al. (2012). Summary report of the geological models transenergy project. Retrieved from http://transenergy-eu.geologie.ac.at/

McPhee, P. J., Koç, A., & van Hinsbergen, D. J. J. (2022). Preparing the ground for plateau growth: Late Neogene Central Anatolian uplift in the context of orogenic and geodynamic evolution since the Cretaceous. *Tectonophysics*, *822*, 229131. https://doi.org/10.1016/j.tecto.2021.229131

Mellere, Stefani, & Angevine. (2000). Polyphase tectonics through subsidence analysis: The Oligo-Miocene Venetian and Friuli Basin, north-east Italy. *Basin Research*, *12*(2), 159–182. https://doi.org/10.1046/j.1365-2117.2000.00120.x

Merlini, S., Doglioni, C., Fantoni, R., & Ponton, M. (2002). Analisi strutturale lungo un profilo geologico tra la linea Fella-Sava e l'avampaese adriatico (Friuli Venezia Giulia-Italia). *Mem. Soc. Geol. It.*, *57*, 293–300.

Mitterbauer, U., Behm, M., Brückl, E., Lippitsch, R., Guterch, A., Keller, G. R., et al. (2011). Shape and origin of the East-Alpine slab constrained by the ALPASS teleseismic model. *Tectonophysics*, *510*(1–2), 195–206. https://doi.org/10.1016/j.tecto.2011.07.001

Most, P. (2003). *Late Alpine cooling histories of tectonic blocks along the central part of the transalp traverse (Inntal—Gadertal): Constraints from geochronology*. Eberhardt-Karls-Universität Tübingen.

Moulin, A., & Benedetti, L. (2018). Fragmentation of the Adriatic promontory: New chronological constraints from Neogene shortening rates across the southern Alps (NE Italy). *Tectonics*, *37*(9), 3328–3348. https://doi.org/10.1029/2018TC004958

Moulin, A., Benedetti, L., Rizza, M., Jamšek Rupnik, P., Gosar, A., Bourlès, D., et al. (2016). The Dinaric fault system: Large-scale structure, rates of slip, and Plio-Pleistocene evolution of the transpressive northeastern boundary of the Adria microplate. *Tectonics*, *35*(10), 2258–2292. https://doi.org/10.1002/2016TC004188

Mroczek, S., Tilmann, F., Pleuger, J., Yuan, X., & Heit, B. (2023). Investigating the Eastern Alpine–Dinaric transition with teleseismic receiver functions: Evidence for subducted European crust. *Earth and Planetary Science Letters*, *609*, 118096. https://doi.org/10.1016/j.epsl.2023.118096

Nussbaum, C. (2000). Neogene tectonics and thermal maturity of the easternmost southern Alps (Friuli area, Italy) [Doctoral Thesis]. Université de Neuchâtel.

Oldow, J. S., Channell, J. E. T., Catalano, R., & D'Argenio, B. (1990). Contemporaneous thrusting and large-scale rotations in the western Sicilian fold and thrust belt. *Tectonics*, *9*(4), 661–681. https://doi.org/10.1029/TC009i004p00661

Ortner, H., Aichholzer, S., Zerlauth, M., Pilser, R., & Fügenschuh, B. (2014). Geometry, amount, and sequence of thrusting in the Subalpine Molasse of western Austria and southern Germany, European Alps. *30*.

Ortner, H., Reiter, F., & Brandner, R. (2006). Kinematics of the Inntal shear zone–sub-Tauern ramp fault system and the interpretation of the TRANSALP seismic section, Eastern Alps, Austria. *Tectonophysics*, *414*(1–4), 241–258. https://doi.org/10.1016/j.tecto.2005.10.017

Ortner, H., von Hagke, C., Sommaruga, A., Mock, S., Mosar, J., Hinsch, R., & Beidinger, A. (2022). The northern deformation front of the European Alps. In C. Rosenberg & N. Bellahsen (Eds.), *Geodynamics of the Alps 3*. ISTE-Wiley.

Paffrath, M., Friederich, W., Schmid, S. M., & Handy, M. R., & the AlpArray and AlpArray-Swath D Working Group. (2021). Imaging structure and geometry of slabs in the greater Alpine area – A P-wave travel-time tomography using AlpArray seismic network data [Data]. *Solid Earth*, *12*(11), 2671–2702. https://doi.org/10.5194/se-12-2671-2021

Pfiffner, O. A. (1993). The structure of the Helvetic nappes and its relation to the mechanical stratigraphy. *Journal of Structural Geology*, *15*(3–5), 511–521. https://doi.org/10.1016/0191-8141(93)90145-Z

Picotti, V., Prosser, G., & Castellarin, A. (1995). *Structures and kinematics of the Giudicarie-Val Trompia fold and thrust belt (central southern Alps, northern Italy)* (Vol. 47). University of Padova.

Picotti, V., Romano, M. A., Ponza, A., Guido, F. L., & Peruzza, L. (2022). The Montello thrust and the active mountain front of the eastern southern Alps (Northeast Italy). *Tectonics*, *41*(12). https://doi.org/10.1029/2022TC007522

Poli, M. E., & Zanferrari, A. (2018). The seismogenic sources of the 1976 Friuli earthquakes: A new seismotectonic model for the Friuli area. https://doi.org/10.4430/bgta0209

Pomella, H., Flöss, D., Speckbacher, R., Tropper, P., & Fügenschuh, B. (2016). The western end of the Eoalpine high-pressure belt (Texel unit, south Tyrol/Italy). *Terra Nova*, *28*(1), 60–69. https://doi.org/10.1111/ter.12191

Pomella, H., Klötzli, U., Scholger, R., Stipp, M., & Fügenschuh, B. (2011). The Northern Giudicarie and the Meran-Mauls fault (Alps, Northern Italy) in the light of new paleomagnetic and geochronological data from boudinaged Eo-/Oligocene tonalites. *International Journal of Earth Sciences*, *100*(8), 1827–1850. https://doi.org/10.1007/s00531-010-0612-4

Pomella, H., Stipp, M., & Fügenschuh, B. (2012). Thermochronological record of thrusting and strike-slip faulting along the Giudicarie fault system (Alps, Northern Italy). *Tectonophysics*, *579*, 118–130. https://doi.org/10.1016/j.tecto.2012.04.015

Ponton, M. (2010). Architettura delle Alpi Friulane. *Museo Friulano di Storia Narturale*. Retrieved from https://arts.units.it/handle/11368/2309482?mode=complete

Ratschbacher, L., Frisch, W., Linzer, H.-G., & Merle, O. (1991). Lateral extrusion in the eastern Alps, Part 2: Structural analysis. *Tectonics*, *10*(2), 257–271. https://doi.org/10.1029/90TC02623

Ratschbacher, L., Frisch, W., Neubauer, F., Schmid, S. M., & Neugebauer, J. (1989). Extension in compressional orogenic belts: The eastern Alps. *Geology*, *17*(5), 404. https://doi.org/10.1130/0091-7613(1989)017<0404:EICOBT>2.3.CO;2

Reid, M. R., Schleiffarth, W. K., Cosca, M. A., Delph, J. R., Blichert-Toft, J., & Cooper, K. M. (2017). Shallow melting of MORB -like mantle under hot continental lithosphere, C entral A natolia. *Geochemistry, Geophysics, Geosystems*, *18*(5), 1866–1888. https://doi.org/10.1002/2016GC006772

Robl, J., Stüwe, K., Hergarten, S., & Evans, L. (2008). Extension during continental convergence in the Eastern Alps: The influence of orogen-scale strike-slip faults. *Geology*, *36*(12), 963. https://doi.org/10.1130/G25294A.1

Rosenberg, C. L., & Kissling, E. (2013). Three-dimensional insight into Central-Alpine collision: Lower-plate or upper-plate indentation? *Geology*, *41*(12), 1219–1222. https://doi.org/10.1130/G34584.1

Rosenberg, C. L., Schneider, S., Scharf, A., Bertrand, A., Hammerschmidt, K., Rabaute, A., & Brun, J.-P. (2018). Relating collisional kinematics to exhumation processes in the Eastern Alps. *Earth-Science Reviews*, *176*, 311–344. https://doi.org/10.1016/j.earscirev.2017.10.013

Royden, L., & Burchfiel, B. C. (1989). Are systematic variations in thrust belt style related to plate boundary processes? (The western Alps versus the Carpathians). *Tectonics*, *8*(1), 51–61. https://doi.org/10.1029/TC008i001p00051

Scharf, A., Handy, M. R., Favaro, S., Schmid, S. M., & Bertrand, A. (2013). Modes of orogen-parallel stretching and extensional exhumation in response to microplate indentation and roll-back subduction (Tauern Window, Eastern Alps). *International Journal of Earth Sciences*, *102*(6), 1627–1654. https://doi.org/10.1007/s00531-013-0894-4

Schlunegger, F., & Castelltort, S. (2016). Immediate and delayed signal of slab breakoff in Oligo/Miocene Molasse deposits from the European Alps. *Scientific Reports*, *6*(1), 31010. https://doi.org/10.1038/srep31010

Schlunegger, F., & Kissling, E. (2022). Slab load controls beneath the Alps on the source-to-sink sedimentary pathways in the Molasse basin [Other]. *display*. https://doi.org/10.5194/egusphere-egu22-3801

Schmid, S. M., Fugenschuh, B., Kissling, E., & Schuster, R. (2004). Tectonic map and overall architecture of the Alpine orogen. *Eclogae Geologicae Helvetiae*, *97*(1), 93–117. https://doi.org/10.1007/s00015-004-1113-x

Schmid, S. M., Pfiffner, O. A., Froitzheim, N., Schönborn, G., & Kissling, E. (1996). Geophysical-geological transect and tectonic evolution of the Swiss-Italian Alps. *Tectonics*, *15*(5), 1036–1064. https://doi.org/10.1029/96TC00433

Schmid, S. M., Scharf, A., Handy, M. R., & Rosenberg, C. L. (2013). The Tauern window (eastern Alps, Austria): A new tectonic map, with cross-sections and a tectonometamorphic synthesis. *Swiss Journal of Geosciences*, *106*(1), 1–32. https://doi.org/10.1007/s00015-013-0123-y

Schönborn, G. (1992). Alpine tectonics and kinematic models of the central southern Alps. *Memorie Degli Istituti Di Geologia e Mineralogia Dell'Universita Di Padova, XLIV*, 229–393.

Schönborn, G. (1999). Balancing cross sections with kinematic constraints: The Dolomites (northern Italy). *Tectonics*, *18*(3), 527–545. https://doi.org/10.1029/1998TC900018

Schuster, R., Kollerm, F., Hoeck, V., Hoinkes, G., & Bousquet, R. (2004). Explanatory notes to the map: Metamorphic structure of the Alps—Metamorphic evolution of the eastern Alps. *Mitteilungen Der Österreichischen Mineralogischen Gesellschaft*, *149*, 71–95.

Selverstone, J. (1993). Micro-to macroscale interactions between deformational and metamorphic processes, Tauern Window, Eastern Alps [Text/html,application/pdf,text/html]. https://doi.org/10.5169/SEALS-55571

Serretti, P., & Morelli, A. (2011). Seismic rays and traveltime tomography of strongly heterogeneous mantle structure: Application to the Central Mediterranean: Traveltime tomography of mantle structure. *Geophysical Journal International*, *187*(3), 1708–1724. https://doi.org/10.1111/j.1365-246X.2011.05242.x

Sinclair, H. D. (1997). Tectonostratigraphic model for underfilled peripheral foreland basins: An Alpine perspective. *Geological Society of America Bulletin*, *109*(3), 0324. https://doi.org/10.1130/0016-7606(1997)109<0324:TMFUPF>2.3.CO;2

Spada, M., Bianchi, I., Kissling, E., Agostinetti, N. P., & Wiemer, S. (2013). Combining controlled-source seismology and receiver function information to derive 3-D Moho topography for Italy. *Geophysical Journal International*, *194*(2), 1050–1068. https://doi.org/10.1093/gji/ggt148

Steenken, A., Siegesmund, S., Heinrichs, T., & Fügenschuh, B. (2002). Cooling and exhumation of the Rieserferner Pluton (eastern Alps, Italy/Austria). *International Journal of Earth Sciences*, *91*(5), 799–817. https://doi.org/10.1007/s00531-002-0260-4

Stöckhert, B., Brix, M. R., Kleinschrodt, R., Hurford, A. J., & Wirth, R. (1999). Thermochronometry and microstructures of quartz—A comparison with experimental flow laws and predictions on the temperature of the brittle–plastic transition. *Journal of Structural Geology*, *21*(3), 351–369. https://doi.org/10.1016/S0191-8141(98)00114-X

Stüwe, K., Robl, J., Plan, L., Fabel, D., Stuart, F., & Gradwohl, G. (2024). The rapid surface uplift of the Eastern Alps. Evidence from cosmogenic nuclides and mapping of elevated low relief surfaces. https://doi.org/10.5194/egusphere-egu24-6089

Tesauro, M., Kaban, M. K., & Cloetingh, S. A. P. L. (2008). EuCRUST-07: A new reference model for the European crust. *Geophysical Research Letters*, *35*(5), 2007GL032244. https://doi.org/10.1029/2007GL032244

TRANSALP Working Group, Gebrande, H., Lüschen, E., Bopp, M., Bleibinhaus, F., Lammerer, B., et al. (2002). First deep seismic reflection images of the Eastern Alps reveal giant crustal wedges and transcrustal ramps. *Geophysical Research Letters*, *29*(10). https://doi.org/10.1029/2002GL014911

Ustaszewski, K., Schmid, S. M., Fügenschuh, B., Tischler, M., Kissling, E., & Spakman, W. (2008). A map-view restoration of the Alpine-Carpathian-Dinaridic system for the Early Miocene. *Swiss Journal of Geosciences*, *101*(S1), 273–294. https://doi.org/10.1007/s00015-008-1288-7

Van Der Meer, D. G., Van Hinsbergen, D. J. J., & Spakman, W. (2018). Atlas of the underworld: Slab remnants in the mantle, their sinking history, and a new outlook on lower mantle viscosity. *Tectonophysics*, *723*, 309–448. https://doi.org/10.1016/j.tecto.2017.10.004

Verwater, V. F., Le Breton, E., Handy, M. R., Picotti, V., Jozi Najafabadi, A., & Haberland, C. (2021). Neogene kinematics of the Giudicarie Belt and eastern Southern Alpine orogenic front (northern Italy). *Solid Earth*, *12*(6), 1309–1334. https://doi.org/10.5194/se-12-1309-2021

Viola, G., Mancktelow, N. S., & Seward, D. (2001). Late Oligocene-Neogene evolution of Europe-Adria collision: New structural and geochronological evidence from the Giudicarie Fault system (Italian eastern Alps). *Tectonics*, *20*(6), 999–1020. https://doi.org/10.1029/2001TC900021

von Blanckenburg, F., & Davies, J. H. (1995). Slab breakoff: A model for syncollisional magmatism and tectonics in the Alps. *Tectonics*, *14*(1), 120–131. https://doi.org/10.1029/94TC02051

Wagner, T., Fabel, D., Fiebig, M., Häuselmann, P., Sahy, D., Xu, S., & Stüwe, K. (2010). Young uplift in the non-glaciated parts of the Eastern Alps. *Earth and Planetary Science Letters*, *295*(1–2), 159–169. https://doi.org/10.1016/j.epsl.2010.03.034

Wagreich, M., & Faupl, P. (1994). Palaeogeography and geodynamic evolution of the Gosau Group of the northern Calcareous Alps (late Cretaceous, eastern Alps, Austria). *20*.

Winterer, E. L., & Bosellini, A. (1981). Subsidence and Sedimentation on Jurassic passive continental margin, southern Alps, Italy. *AAPG Bulletin*, *65*, 394–421.

Wolff, R., Hetzel, R., Dunkl, I., & Anczkiewicz, A. A. (2021). New constraints on the exhumation history of the western Tauern Window (European Alps) from thermochronology, thermokinematic modeling, and topographic analysis. *International Journal of Earth Sciences*, *110*(8), 2955–2977. https://doi.org/10.1007/s00531-021-02094-w

Wölfler, A., Kurz, W., Fritz, H., & Stüwe, K. (2011). Lateral extrusion in the Eastern Alps revisited: Refining the model by thermochronological, sedimentary, and seismic data. *Tectonics*, *30*(4), 2010TC002782. https://doi.org/10.1029/2010TC002782

Wölfler, A., Stüwe, K., Danišík, M., & Evans, N. J. (2012). Low temperature thermochronology in the Eastern Alps: Implications for structural and topographic evolution. *Tectonophysics*, *541–543*, 1–18. https://doi.org/10.1016/j.tecto.2012.03.016

Wortel, M. J. R., & Spakman, W. (2000). Subduction and slab detachment in the Mediterranean-Carpathian region. *Science*, *290*(5498), 1910–1917. https://doi.org/10.1126/science.290.5498.1910

Zanferrari, A., Masetti, D., Monegato, G., & Poli, M. E. (2013). *Carta Geologica d'Italia 1:50000, Sheet 49 – Gemona Del Friuli [Map]*. ISPRA - Servizio Geologico d'Italia.

Zhu, H., Bozdağ, E., & Tromp, J. (2015). Seismic structure of the European upper mantle based on adjoint tomography. *Geophysical Journal International*, *201*(1), 18–52. https://doi.org/10.1093/gji/ggu492

Žibret, L., & Žibret, G. (2023). Neogene block rotation inside the dextral fault zone at the Adriatic-European collision zone: Reexamination of existing results. *Journal of Asian Earth Sciences*, *254*, 105723. https://doi.org/10.1016/j.jseaes.2023.105723

Zingg, A., Handy, M. R., Hunziker, J. C., & Schmid, S. M. (1990). Tectonometamorphic history of the Ivrea zone and its relationship to the crustal evolution of the southern Alps. *The Nature of the Lower Continental Crust*, *182*(1), 169–192. https://doi.org/10.1016/0040-1951(90)90349-D